Dynamics of Synaptic Transmission in the CNS:

Contribution of Neuron-Glia interactions

Jaekwang Lee

A dissertation submitted to the faculty of the University of North Carolina at Chapel Hill in partial fulfillment of the requirements for the degree of Doctor of Philosophy in the Department of Biomedical Engineering.

Chapel Hill
2010

Approved by:

Barry Whitsel

Bob Dennis

Jeff MacDonald

Mark Tommerdahl

Oleg Favorov

ABSTRACT

JAEKWANG LEE: Dynamics of Synaptic Transmission in the CNS: Contribution of Neuron-Glia interactions.

(Under the direction of Mark Tommerdahl)

ABSTRACT

The last 30 years have seen a growing appreciation of the importance for CNS functioning of the internal state of neural tissues, which is exquisitely reflective of the immediate-to-long-term history of the preceding neural activity experienced by those tissues. This dissertation comprises three research projects that together address different, but related aspects of dynamics of the state of neural tissues, with a focus on the roles played by astroglia and GABAergic synaptic transmission. The first two projects study the relationship between stimulus-evoked glial and neuronal activities within local networks of the dorsal horn of the spinal cord and sensitivity of GABAergic actions to the state of local glia and prior sensory stimulation, whereas the third project investigates the sensitivity of GABAergic actions to prior sensory stimulation in the neocortex.

Project 1: Origins of Optical Intrinsic Signal and its significance. In rat spinal cord slice, repetitive electrical stimulation of the dorsal root at an intensity that activates C-fibers evokes a slow-to-develop and prolonged (30–50 s) change in light transmittance (OIS_{DR}) in the

superficial part of the ipsilateral dorsal horn (DHs). Inhibition of astrocyte metabolism by bath-applied fluoroacetate and glutamine (FAc+Gln), or interference with glial and neuronal K^+ transport by 4-aminopyridine (4-AP) lead to dissociation of the OIS_{DR} and the postsynaptic DHs response to a single-pulse dorsal root stimulus ($P\text{-}PSP_{DR}$). The OIS_{DR} decreases under FAc+Gln, whereas the $P\text{-}PSP_{DR}$ remains unaltered; under 4-AP, the $P\text{-}PSP_{DR}$ increases, but the OIS_{DR} decreases. In contrast, both the OIS_{DR} and $P\text{-}PSP_{DR}$ increase when K^+_o is elevated. These observations indicate that the OIS_{DR} mainly reflects cell volume and light scattering changes associated with DHs astrocyte uptake of K^+ and glutamate (GLU). In slices from subjects that received an intracutaneous injection of formalin 3–5 days earlier, both the OIS_{DR} and the response of the DHs to local application of K^+ or GLU are profoundly reduced, and the normally exquisite sensitivity of the DHs to elevated K^+o is decreased. Considered collectively, the observations raise the possibility that impaired regulation of DHs K^+_o and GLUo may contribute to initiation and maintenance of the CNS pain circuit and sensorimotor abnormalities that develop following intracutaneous formalin injection.

Project 2: Effects of alteration of glia on neuronal plasticity. Transient (20min) exposure of the spinal cord slice to fluorocitrate (FC; a reversible inhibitor of glial energy production via the TCA cycle) is shown to be accompanied by a protracted *decrease* of the superficial dorsal horn (DH_s) optical response to repetitive electrical stimulation of the ipsilateral dorsal root, and by a similarly protracted *increase* in the postsynaptic response of the DH_s to single-pulse stimulation of the attached dorsal root (LTP_{FC}). It also is shown that LTP_{FC} *does not* occur in the presence of d-aminophosphopentanoic acid (APV), becomes progressively *smaller* as $[K^+]_o$ in the perfusion solution is decreased from 3.0 mM ("normal") to 0.0 mM, and is *reduced* or

eliminated by bath application of 1 mM bicuculline. Somal whole-cell patch recordings were carried out to evaluate the effects of FC on the response of DH_s neurons to puffer-applied GABA. The observations reveal that transient exposure of the slice to FC is reliably accompanied by a prolonged (>1 hr) depolarizing shift of the equilibrium potential for the DH_s neuron transmembrane ionic currents evoked by GABA (average $E_{GABApreFC}$: -75 mV ; $E_{GABApostFC}$: -50 mV). Considered collectively, the findings demonstrate that LTP_{FC} involves (1) elevation of $[K^+]_o$ in the DH_s, (2) NMDA receptor activation, and (3) conversion of the effect of GABA on DH_s neurons from inhibition to excitation. It is proposed that a transient impairment of astrocyte energy production via the TCA cycle can trigger the cascade of dorsal horn mechanisms that underlies hyperalgesia and persistent pain.

Project 3: Contribution of GABA to cerebral cortical dynamics. Imaging of the optical intrinsic signal (OIS), evoked in the rat sensorimotor cortical slice by 1s-long 20Hz electrical stimulation applied to locus at the layer VI/white matter junction, was used to delineate a column-shaped cortical region responding to a local thalamocortical input drive, and whole-cell patch clamp recordings were obtained from layer II-III pyramidal neurons residing in that region. Puffs of pressure-ejected GABA were released from a micropipette in a close vicinity of the recorded neuron's soma before and also immediately after "conditioning" electrical stimulation. Prior to conditioning stimulation, GABA puffs hyperpolarized the recorded neurons, whereas for ~15s subsequent to conditioning stimulation GABA puffs depolarized the same neurons. Two-photon Cl^- imaging in cortical slices taken from CLM1 Clomeleon mice revealed that conditioning stimulation transiently elevates $[Cl^-]_i$ in the stimulated cortical column;

this increase is blocked by SR95531 (gabazine), a selective $GABA_A$ receptor antagonist. Next, two-photon Ca^{2+} imaging revealed that isoguvacine ($GABA_A$ receptor agonist) increases Ca^{2+} influx into neurons in the stimulated cortical column. Finally, OIS imaging in the presence of GABA antagonist bicuculline suggests that the depolarizing action of GABA is confined to the center of the stimulated cortical region, while at its margins GABA remains hyperpolarizing. Taken together, these findings suggest that synaptically released GABA can be either inhibitory or excitatory, depending on the activity state of the local network. Such activity dependence of GABA action can be expected to funnel stimulus-evoked activity in a cortical area into the central, most strongly driven cortical columns.

ACKNOWLEDGEMENTS

I would like to acknowledge all those people who have assisted in the completion of this work. Special thanks go to my colleagues, the members of my committee Barry Whitsel, Bob Dennis, Jeff Macdonald, Mark Tommerdahl, and Oleg Favorv whose guidance and drive have been an inspiration to me.

I also would like to thank my family, specially my spouse Hyesun Cho and son Sun Lee who have given endless supports and strength to me to finish without giving it up. I thank my parents whose pray has been a motivation to me. Most special thanks go to God.

Table of Contents

Table of Figures

Chapter 1

Introduction

The central nervous system (CNS) is a complex nonlinear dynamical system. In the last 30 years there has been a profound evolution of our thinking of CNS from the traditional Sherringtonian view of CNS as a connectionist network organized into a system of reflex arcs, in which external stimulus-triggered activity is propagated through chains of synapses in mostly hard-wired ways to eventual muscle contractions, to a much greater appreciation of the importance for CNS functioning of the internal state of neural tissues, which is exquisitely reflective of the immediate-to-long-term history of the preceding neural activity experienced by those tissues. A great multitude of neural mechanisms have been identified in the last 30 years that control the internal state of neural tissues, from – among other things – short-term spike firing-driven pre- and post-synaptic adaptation at individual synapses to transient changes in excitability of neurons and local neuronal populations to long-term changes in synaptic wiring.

Particularly important for this new appreciation of CNS dynamics is our evolving understanding of glia. Glial cells, such as astrocytes, oligodendrocytes and microglia, are the integral part of CNS and comprise the majority of cells in the brain. Despite their numbers, for a long time their role was thought to be limited to simple supportive function for the neighboring neurons. The most basic role of astrocytes, which are the most abundant type of glial cells, is regulating extracellular space and transport of ions, metabolites and

micromolecules. It is now have become well established that neurons transmit signals to glial cells by releasing K^+ into the intercellular space during nerve activity, simultaneously depolarizing their membrane potential. Glial cells respond to released K^+ by sequestering it, thereby protecting the neurons against perturbations in the extracellular concentration of those ions. Several recent studies have also shown that astrocytes can release a variety of different molecules upon activation by neurotransmitters, which has led to the concept of 'gliotransmission'. Termination of neurotransmission and prevention of neurotransmitter spreading into the extra-synaptic space is achieved by active transport of transmitter molecules, such as glutamate, glycine and γ-amino butyric acid (GABA), d-serine, and ATP into the surrounding neuronal and glial cells through complex transport systems. Glial transport acts as an efficient buffering system for neurotransmitters; however, it has also become clear that glial transport plays a crucial role in shaping synaptic transmission.

Glia also plays a central role in repairing damage to neural tissues. Tissue injury, infection, or inflammation frequently is accompanied by transformation (activation) of the glia in the affected region (e.g., Watkins and Maier 2002). Glial activation involves changes in astrocyte shape and volume and altered communication between neighboring astrocytes via gap junctions (Meme et al. 2004; Olsen and Sontheimer 2004; Walz 2002). Astrocytes in the affected region exhibit decreased expression of glutamate transporters and K_{IR}-type membrane potassium channels (Huang et al. 2004; Kawahara et al. 2002; MacFarlane and Sontheimer 1997; Olsen and Sontheimer 2004), increased Cl^- conductance (Parkerson and Sontheimer 2004; Walz 2002), absence of the $[Ca^{2+}]_i$ transients normally evoked by afferent activity (Aguado et al. 2002), and altered expression of genes regulating production and

release of neuroactive cytokines, chemokines, growth factors, and NO (Meeuwsen et al. 2003; Milligan et al. 2001).

Another potentially important source of short-term dynamics in CNS is the major inhibitory neurotransmitter GABA (γ-aminobutyric acid), which works by binding to ionotropic Cl^- permeable $GABA_A$ receptors and to metabotropic K^+ permeable $GABA_B$ receptors. In immature neurons, GABA is known to exert an excitatory – rather than inhibitory – effect, which is mediated by chloride efflux through $GABA_A$ channels. The principal basis of GABA-mediated excitation involves intracellular chloride ($[Cl^-]_i$) accumulation resulting from the differential expression and activity of the cation chloride co-transporters NKCC1 and KCC2 (Staley,2006). Several studies of neurons in adult hippocampus and neocortex have also identified an activity-dependent conversion of the synaptic action of GABA from hyperpolarizing/inhibitory to depolarizing/excitatory in a healthy, normally functioning cerebral cortex. In addition, an increase in extracellular space K^+ concentration can raise Cl^- reversal potential in neighboring neurons, which is a possible reason that impairment of the ability of astrocytes to regulate extracellular K^+ and glutamate levels may alter GABAergic transmission from inhibitory to excitatory in neuropathological conditions.

This dissertation comprises three research projects that together address different, but related aspects of dynamics of the state of neural tissues, with a focus on the roles played by astroglia and GABAergic synaptic transmission. The first two projects study the relationship between stimulus-evoked glial and neuronal activities within local networks of the dorsal horn of the spinal cord and sensitivity of GABAergic actions to the state of local glia and

prior sensory stimulation, whereas the third project investigates the sensitivity of GABAergic actions to prior sensory stimulation in the neocortex.

Chapter 2

Materials and Methods

2.1 Slice preparation

2.1.1 Spinal cord Slice

The subject was placed in a light-tight enclosure. An anesthetic gas mix (4% halothane in a 50/50 mix of nitrous oxide and oxygen) was delivered to the interior of the enclosure via a tube connected to an anesthesia machine (COMPAC-50, Forreger). After induction of general anesthesia, ketamine was administered intraperitoneally (0.5 ml of a 25 mg/ml solution) to prevent CNS excitotoxicity. Local anesthetic (lidocaine; 0.1–0.2 ml of a 1 mg/ml solution) was injected into the paravertebral musculature at three to four equally spaced sites on both sides of the vertebral column between levels T_5 and S_3 to reduce/eliminate the impact on the lumbosacral spinal cord dorsal horn of the vigorous afferent barrage that otherwise would accompany surgical isolation of the spinal cord and transection of the dorsal roots. After administration of the local anesthetic, the subject was transferred to a bed of ice (to lower body temperature). General anesthesia was maintained by administering the anesthetic gas mix via a face mask, and the vertebral column and spinal cord were excised, placed in ice-cold artificial cerebrospinal fluid (ACSF; NaCl replaced by sucrose), and the lumbosacral cord and attached dorsal roots were freed from surrounding tissues by microdissection.

Transverse slices of the lumbosacral cord (400–800 μm thickness) were cut serially using an oscillating tissue slicer (OTS-4000, Electron Microscopy Sciences) and placed in a reservoir containing ACSF warmed (30°C) and oxygenated (using a 95% O_2-5% CO_2 gas mix). Each slice remained in the reservoir until (never <1 h) it was transferred (by pipette) to the recording chamber. The recording chamber was continuously perfused with warmed (28–30.8°C) and oxygenated ACSF (perfusion rate 1.5–2 ml/min). Composition (in mM) of the ACSF was 124 NaCl, 3.0 KCl, 2.5 $CaCl_2$, 25 $NaHCO_3$, 1 $MgSO_4$, 1.25 NaH_2PO_4, and 10 glucose. A fine nylon mesh stabilized the slice in a submerged position. A total of 233 slices were studied—152 from 67 normal/untreated subjects, and 81 from 36 subjects in which the right hindpaw was injected with formalin 3–5 days before the experiment.

2.1.2 Cortical Slice

Coronal slices (350 - 400μm) were prepared from the sensorimotor cortex of young adult (3-4 weeks old) rats (Sprague–Dawley, Charles River) and mice (B6or homozygous CLM1). Following decapitation, the brain was rapidly removed and placed in ice-cold artificial cerebrospinal fluid (ACSF) having the following composition (in mM): NaCl, 118; KCl, 4.8; $CaCl_2$, 2.5; $NaHCO_3$, 25; $MgSO_4$, 1.2; KH_2PO_4, 1.2; and glucose, 10. Slices were cut using an oscillating tissue slicer (Vibratome 3000, Vibrotome) at 3°C. Slices were stored in a bath of warmed (30°C), oxygenated (95% O_2, 5% CO_2) ACSF for a recovery period of at least 1 h prior to placement in a recording chamber mounted on an upright microscope (BX50WI, Olympus). Slices were submerged in the chamber, and perfused with warmed (28–30°C) oxygenated ACSF at a rate of 1.5–2 ml/min. The composition of the ACSF used in the recording chamber was the same as that in the recovery chamber.

The viability and functional stability of the slice was monitored using evoked potential recordings. A glass micropipette filled with 1M NaCl (impedance 1–2 MΩ) was placed approximately 400μm from the pial surface (layer III). Evoked potentials were band-pass filtered (30–300Hz) and sampled at 20KHz. A threshold stimulus, defined as the minimum current necessary to generate an evoked potential, was determined for each slice; for the data reported in this paper the threshold current ranged from 30 to 50μA.

2.2 Electrophysiology

2.2.1 Field potential recordings

Single-pulse (0.2 ms duration) constant-current stimuli were applied to the peripheral end of the attached dorsal root using a suction electrode, isolation unit, and programmable pulse generator (Master 8, AMPI). The postsynaptic field potential evoked in the DH_s by the dorsal root stimulus ($P\text{-}PSP_{DR}$) was recorded with a 1–2 mM NaCl-containing glass micropipette (shaft 1.2 mm OD; pulled with a vertical puller; Narishige PP-83). Each $P\text{-}PSP_{DR}$ was obtained by placing the tip of the recording micropipette in the substantia gelatinosa (SG; lamina II; all $P\text{-}PSP_{DR}$s were obtained in the region of the SG where the intrinsic signal evoked by the standard repetitive dorsal root stimulus (OIS_{DR}) was maximal and, whenever possible, at a locus where the field potential consisted of clearly separated short- and longer-latency responses to single-pulse stimulation of the dorsal root (Hantman et al. 2004; Lu and Perl 2003; Ruscheweyh and Sandkuhler 2000). $P\text{-}PSP_{DR}$s were evoked using stimulus currents two to four times the minimum (threshold; typically 50–80 μA) current. Currents of this intensity consistently activate both large- (A) and small-diameter (A and C) dorsal root fibers (Asai et al. 2002; Ikeda et al. 1998; Murase et al. 1998, 1999; Ruscheweyh

and Sandkuhler 2000, Ruscheweyh and Sandkuhler 2001). Recordings of P-PSP$_{DR}$s were band-pass filtered (20–500 Hz) and sampled at 20 KHz using pClamp 6.0 (Axon Instruments).

2.2.2 Whole cell patch clamp recordings

In experiments of this type the slice was transferred from the reservoir to the recording chamber of a fixed-stage upright microscope (Olympus BX51WI) and visualized directly via the microscope's optics, or indirectly via a high resolution CCD camera system (CCD-100, Dage-MTI, Inc) that received the output of a CCD camera attached to the microscope's video port. Whole cell patch-clamp recordings were obtained from lamina II neurons using borosilicate glass pipettes (resistance 4 – 6 MOhm) pulled on a 2-stage vertical pipette puller (Narishige PC-10), and filled with a solution with the following composition (in mM): 120.0 K-gluconate, 20.0 KCl, 2.0 $NaCl_2$, 20.0 HEPES, 0.5 EGTA, 10.0 glucose, 2.0 Na-ATP, 0.5 Na-GTP; pH adjusted to 7.3 with KOH. Patch recordings were obtained under the same slice conditions (temperature, perfusion rate, etc.) used to obtain OIS imaging and field potentials observations. Voltage-clamp and current-clamp recordings were carried out with a MultiClamp 700B amplifier, using pClamp9 acquisition software (Molecular Devices, Union City, CA, USA). Signals were filtered at 50-500 Hz, sampled at 5 kHz for identification of cell type and at 50 Hz for the GABA application part of the experiment. Data were analyzed and plotted using Origin 7.0. No correction for liquid junction potential was made. Cells with resting potentials greater than -60 mV or less than -80 mV were regarded as "abnormal" and were not studied further.

Once a neuron was accepted for study the tip of a glass pipette filled with 1 mM GABA was placed (using a 3-axis micropositioner; NMN-25, Narishige Group Inc., Tokyo, Japan) at a location within 50-100 μm of the soma. The GABA equilibrium potential (E_{GABA})

was determined by measuring the transmembrane current evoked by a temporally controlled, local application of GABA (a 300 msec "puff" delivered at 3-5 psi via the pipette filled with 1 mM GABA; using Picospritzer II, Parker Hannifin Corp.) at holding potentials ranging between -100 mV and -20 mV (step size = 20 mV), both before and after exposure of the slice to FC. Each GABA puff applied during the study of a neuron was delivered at the same location in the DH_s, and at the same pressure and duration.

2.3 Imaging

2.3.1 Optical Intrinsic Signal recordings

The submerged slice was transilluminated using a controlled light source (Oriel), and images were obtained at x2 or x4 magnification using an inverted microscope (Diaphot 200, Nikon) and a cooled, slow-scan CCD camera (Photometrics). The optical response of each slice to a standard dorsal root stimulus consisting of a series of repetitive constant-current pulses (pulse duration, 0.2 ms; 2–4 times the intensity at which an optical response was first detected; train duration, 1.0 s; frequency, 20 Hz) was recorded. The standard stimulus was applied once every 30 s to the attached root at the dorsal root entry zone using a 50-μm-diam bipolar stimulating electrode, isolation unit, and programmable pulse generator (Master-8, AMPI).

The imaged region of each slice was extensive: it always included all layers of the dorsal horn on one side and much of the neighboring ventral horn and white matter on the same side. The region of an image evaluated using quantitative analytical approaches was selected using a criterion independent of investigator interest/bias—i.e., the evaluated region always was the region that underwent an increase in light transmittance [the optical intrinsic

signal (OIS)] (Asai et al. 2002; Murase et al. 1999, 1998; Sykova et al. 2003) in response to the standard dorsal root stimulus. In every slice, the evaluated region was confined to the superficial dorsal horn (DH_s; i.e., layers I, II_o, and II_i).

The OIS not only develops in CNS regions in which a stimulus evokes increased spike discharge activity, but also in regions in which neurons undergo subthreshold decreases in membrane potential [i.e., excitatory postsynaptic potentials (EPSPs) without action potentials] (Kohn et al. 2002a,b; Shoham and Grinvald 2001). These attributes, together with its high spatial and temporal resolution, make the OIS imaging method well suited for detection, localization, and quantification of the population-level responses of the dorsal horn to both electrical stimulation of the dorsal root and direct application (using a puffer pipette) of neuroactive chemicals.

A series of 30 images was acquired (image acquisition rate = 0.5/s) in a fixed temporal relationship to each application of the standard dorsal root stimulus (a trial). The first and second images in such a trial were obtained at 1000 ms and at 500 ms before stimulus onset (reference images); two poststimulus onset images were obtained during the standard stimulus and the remaining 26 images after termination of the stimulus. Trial duration was 15 s. An average difference image was generated from the images acquired during each trial. Each average difference image was formed by *1*) subtracting the reference image obtained at 500 ms before stimulus/puff onset from each image obtained in the same trial between 2.5 and 12.5 s after stimulus/puff onset (images 6–25; total of 20), and *2*) at each pixel location by dividing the sum of the differences between the poststimulus/postpuff and reference images (same-trial) by the number of frames (20). An intensity value was calculated for each pixel in a difference image using the formula [sumn]$(T_{ij} - T_{i,ref})/T_{i,ref}$,

where T_{ij} is the intensity of the ith pixel in the jth image, and $T_{i,ref}$ is the intensity of the ith pixel in the reference image. The same approach was used to evaluate series of images acquired before, during, and after a brief, local application of either 15 mM K^+ or 100 μM glutamate (GLU; using a puffer pipette and controlling electronics; Picospritzer II, General Valve).

Mean intensity (T/T) of either the OIS_{DR} or the optical response to puffer-applied K^+ or GLU was determined by *1*) bounding the region in the DH_s that the transmittance values met or exceeded a criterion increase in transmittance (typically the upper 5–10% of pixel values in the image), and *2*) computing the average intensity of all pixels within the bounded region. The effect of a treatment (e.g., bath-applied local anesthetic) on the mean intensity of the OIS_{DR} or the response to puffer-applied GLU or K^+ was quantified as follows. The same region of the DH_s used to determine T/T for the control response also was used to measure T/T for the response obtained under the treatment condition. Treatment effect was expressed in terms of the mean intensity of the control response: i.e., $T/T_{treatment}/T/T_{control}$ x 100 = %. All average difference images shown in this paper were contrast enhanced using a standard histogram equalization procedure.

2.3.2 Two photon microscopy for Cl^- and Ca^{2+} imaging

A customized 2-photon microscopy system (TrimScope, LaVisionBioTec, Bielefeld, Germany) was used to visualize stimulus-evoked intracellular Cl^- change in somatosensory cortical slices obtained from Cloemeleon mice (homozygous CLM1 mice; Beglund et al., 2008) and intracellular Ca^{2+} changes in B6 mice. Upright microscope (Olympus BX51 WI, Japan) equipped with a 203 water immersion lens (0.95 W, XLUMPlanFI, Olympus,

Germany) was used for ratiometric Cl^- and Ca^{2+} imaging. The excitation source was a mode-locked Ti/Sapphire laser (Mai Tai; Spectra Physics, Santa Clara, CA) tuned to 800nm. The imaging software (Imspector Pro; LaVisionBioTec, Bielefeld, Germany) allows simultaneous recordings of two fluorescent signals (CFP filter: 500 SP; YFP filter: 535 BP 50) as fluorescence resonance energy transfer (FRET) signals. For Cl^- imaging, time series of images were acquired from Clomeleon-expressing cells. Various image geometries (64×8 to 256×256 pixels) with a scan rate of 2ms/line (=62.5 to 2 frames/s) were used. The data were analyzed offline with MetaMorph version 7.6 (Moleculardevices, Sunnyvale, CA) and Matlab software.

To measure Ca^{2+} signals, slices were transferred to microscope after incubation with 5μmol/L Fura-2 AM plus 1μmol/L pluronic acid (Molecular Probes) for 30min at room temperature. External solution for dye staining contained 150mmol/L of NaCl, 10mmol/L of HEPES, 3mmol/L of KCl, 2mmol/L of $CaCl_2$, 1 mmol/L of $MgCl_2$, 22 mmol/L of sucrose, and 10 mmol/L of glucose (pH adjusted to 7.4 and osmolarity to 325mOsm). Under 2-photon microscope, the laser was tuned to 810nm. Recordings of signal intensity and conversion to $[Ca^{2+}]$ were performed by MetaMorph version 7.6 (Moleculardevices) and Matlab software.

Chapter 3

Origins of Optical Intrinsic Signal and its significance

3.1 Background

Tissue injury, infection, or inflammation frequently is accompanied by transformation (activation) of the glia in the topographically corresponding region of the spinal cord dorsal horn (Watkins and Maier 2002). Glial activation involves changes in astrocyte shape and volume and altered communication between neighboring astrocytes via gap junctions (Meme et al. 2004; Olsen and Sontheimer 2004; Walz 2002). Astrocytes in the affected region of the dorsal horn exhibit increased expression of glial fibrillary acidic protein (GFAP) (Garrison et al. 1994), decreased expression of glutamate transporters and K_{IR}-type membrane potassium channels (Huang et al. 2004; Kawahara et al. 2002; MacFarlane and Sontheimer 1997; Olsen and Sontheimer 2004), increased Cl^- conductance (Parkerson and Sontheimer 2004; Walz 2002), absence of the $[Ca^{2+}]_i$ transients normally evoked by afferent activity (Aguado et al. 2002), and altered expression of genes regulating production and release of neuroactive cytokines, chemokines, growth factors, and NO (Meeuwsen et al. 2003; Milligan et al. 2001).

Application of algesic chemical to skin or muscle not only is followed by glial activation in the dorsal horn region that receives afferent projections from the tissue exposed to the chemical, but also by hyperalgesia/persistent pain and abnormal pain-related sensorimotor behaviors (Banna et al. 1986; Dickenson and Sullivan 1987; Fu et al. 2000;

Porro and Cavazzuti 1993; Watkins and Maier 2002; Watkins et al. 1997). Moreover, the intensity and time-course of dorsal horn glial activation are strongly correlated with the pain-related sensorimotor behaviors triggered by the exposure to algesic chemical (Watkins and Maier 2002; Watkins et al. 1997), and neurons in the region of the horn that receives input from the exposed tissue display unusual receptive field and response properties consistent with subjects' abnormal pain-related sensorimotor behaviors (Watkins and Maier 2002; Woolf and Salter 2000).

Although it is established that the morphological, biochemical, and functional properties of the glia of the dorsal horn modify after exposure of skin or muscle to an algesic chemical, the relationship between the glial alterations and the neuronal/perceptual abnormalities that develop after such an exposure is incompletely understood. This gap in understanding motivated us to investigate the effects on the dorsal horn of intracutaneous injection of 5% formalin. Our primary goal was to evaluate whether the glial activation that follows intracutaneous injection of formalin is accompanied by significant modification of the normally appreciable ability of astrocytes to homeostatically regulate local extracellular fluid composition. We regarded multiple lines of published evidence as consistent with the possibility that the vigorous C-nociceptor activity evoked by algesic chemical to skin or muscle (Klemm et al. 1989; McCall et al. 1996; Porro et al. 2003; Puig and Sorkin 1996) is accompanied by an impaired ability of astrocytes to regulate dorsal horn extracellular fluid composition. First, intracutaneous formalin injection is accompanied by a large and prolonged elevation of $[K^+]_o$ in the superficial dorsal horn (Heinemann et al. 1990; Svoboda et al. 1988). Second, tetanic nerve stimulation, noxious skin stimulation, inflammation, or an experimentally imposed elevation of dorsal horn $[K^+]_o$ is followed by long-term changes in

the efficacy of C-fiber–mediated synaptic activation of dorsal horn neurons (Ma et al. 2002; Sandkuhler and Liu 1998; Sandkuhler et al. 2000; for CNS effects of elevated $[K^+]_o$, see Somjen 2002). Third, the hyperalgesia/persistent pain, glial activation, and the abnormal elevation of dorsal horn $[K^+]_o$ that develop after intracutaneous formalin injection are either prevented entirely or substantially reduced by prior local anesthetic block of action potential conduction in the afferents that innervate the injection site (Fu et al. 2000; Svoboda et al. 1988).

The optical imaging and neurophysiological observations reported in this paper strongly suggest that 3–5 days after intracutaneous injection of formalin astrocyte, regulation of $[K^+]_o$ and $[GLU]_o$ is profoundly impaired in the region of the dorsal horn that receives direct afferent input from the injected skin site. The findings raise the possibility that impaired astrocyte regulation of the extracellular fluid composition contributes to the establishment of the dorsal horn neuronal circuit abnormalities that underlie hyperalgesia/persistent pain. Some of the results were described in a preliminary communication (Lee et al. 2003)

3.2 Results

3.2.1 Studies of slices from untreated (control) subjec Figure 4.3.1ts

3.3.1.1 OIS_{DR} DEPENDS ON STIMULUS-EVOKED NEUROTRANSMISSION. Figure 4.3.1 summarizes results obtained from two of the six slices in which the dependency of the OIS_{DR} on neurotransmission was evaluated. The *top left* image in Fig. 3.1, *A* and *B*, is a reference image that shows the superficial dorsal horn (DH_s) and several of the bordering anatomical structures (e.g., DC, dorsal column; LC, lateral column; VH, ventral horn). Comparison of

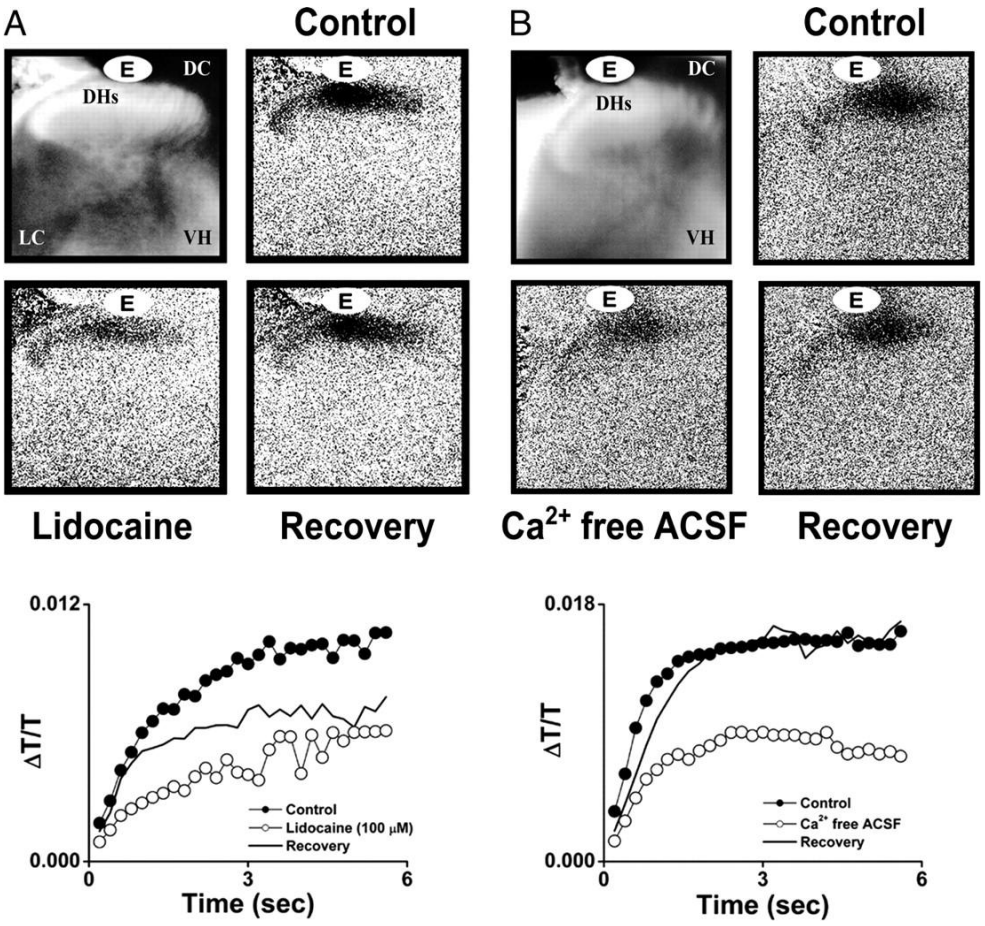

Figure 3. 1. Dependency of light transmittance (OIS_{DR}) on neurotransmission. ***A*****:** effect of lidocaine. ***B*****:** effect of 0 Ca^{2+}. *Top left* in *A* and *B*: reference image in which superficial dorsal horn (DH_s = layers I, II_o, and II_i) and ventral horn (VH) appear white; heavily myelinated regions [e.g., the dorsal (DC) and lateral columns (LC)] appear black. Oval containing label "E" indicates position of stimulating electrode. Grayscale images in *A* and *B*: prestimulus – poststimulus difference images showing OIS_{DR} under control condition (Control), during exposure to 100 μM lidocaine (Lidocaine) or 0 Ca^{2+} artificial cerebrospinal fluid (ACSF; Ca^{2+}-free ACSF), and after return of perfusate to normal ACSF (Recovery). Region of slice in which light transmittance increased in response to dorsal root stimulation (dark pixels) corresponds to the DH_s. Pixel size (spatial resolution) = 7 μm. *T*/*T* vs. time plots at *bottom* show time course of stimulus-evoked increase in transmittance (0 point on abscissa indicates time of stimulus onset) under each control, treatment, and recovery condition.

each reference image with the corresponding prestimulus – poststimulus difference images (images at *top right* and *bottom right* in Fig. 3.1, *A* and *B*) shows that in both slices *1*) the region in the slice that undergoes an increase in transmittance in response to dorsal root stimulation lies within the boundaries of the DH_s, and *2*) the stimulus-evoked increase in transmittance (OIS_{DR}) is substantially reduced when the ACSF contains either 100 μM

lidocaine (compare control vs. lidocaine images in Fig. 3.1*A*)—lidocaine at this concentration blocks action potential conduction in excitable tissue—or lacks Ca^{2+} (control vs. Ca^{2+}-free ACSF in Fig. 3.1*B*). Ca^{2+}-free ACSF reduces transmitter release from the presynaptic terminals of dorsal root afferents. Figure 4.3.1 also shows that the OIS_{DR} recovers to near control values 30–60 min after the fluid perfusing the recording chamber is returned to drug-free ACSF. On average, bath- applied 100 μM lidocaine reduced the OIS_{DR} to 37.74 ± 9.13% of control ($P < 0.003$; $n = 3$ slices); and zero Ca^{2+} ACSF reduced the OIS_{DR} to 53.42 ± 1.28% of control ($P < 0.001$; $n = 3$ slices). The T/T versus time plots at the *bottom* of Fig. 3.1 show that at times between 200 ms and 6 s after stimulus onset, ACSF containing 100 μM lidocaine or lacking Ca^{2+} consistently suppressed the transmittance increase elicited by dorsal root stimulation.

3.2.2 Temporal properties of the OIS_{DR}

While the effects of local anesthetic and Ca^{2+}-free ACSF show that the OIS_{DR} depends on stimulus-evoked neurotransmission, the slow temporal properties of the OIS_{DR} clearly differentiate it from stimulus-evoked dorsal horn neuroelectrical activity. The T/T versus time plots in Fig. 3.2 (*bottom right*) show the time-course of the OIS_{DR} at three different loci within the same dorsal horn. These plots show that *1*) the magnitude of the stimulus-evoked transmittance increase was largest at DH_s site 1, intermediate at site 2, and smallest at site 3, and *2*) at each site, the stimulus-evoked increase in transmittance continued at near-maximal values for a prolonged period after stimulus termination. Although the T/T versus time plots are truncated at 6 s after stimulus onset, transmittance at site 3 (the site at which the OIS_{DR} was weakest) remained above background for 20 s after stimulus termination and above

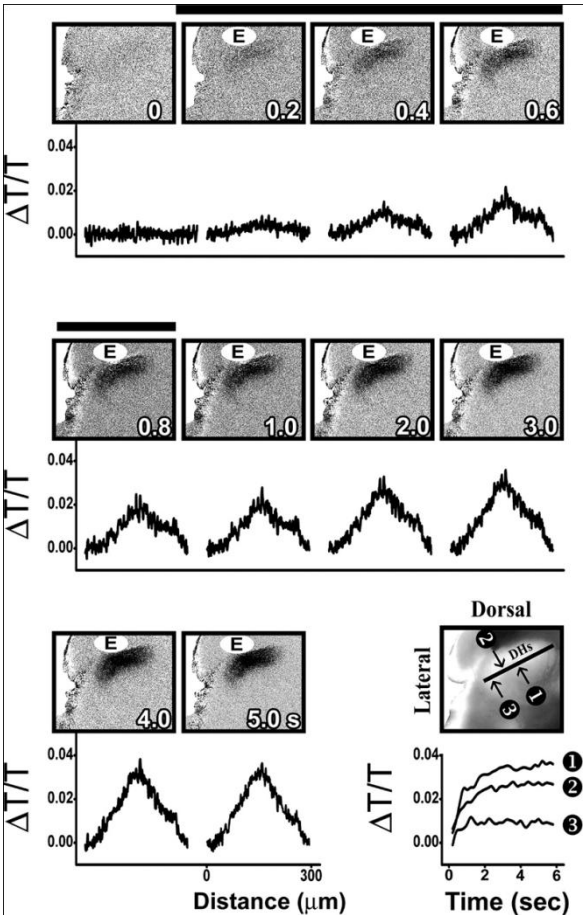

Figure 3. 2. **Spatial and temporal characteristics of the OIS_{DR}.** Sequence of difference images obtained between 0.0 and 5.0 s after stimulus onset. Bar at *top* between 0.2 and 0.8 s indicates period during which repetitive dorsal root stimulus was applied. Plots at *bottom right* show time dependency of OIS_{DR} at each of 3 sites within the DH_s (sites indicated by arrows in reference image at *bottom right*). Plot of T/T vs. distance below each difference image shows spatial distribution of transmittance increase along mediolateral path within the DH_s (path indicated by bar drawn through DH_s in reference image). T/T vs. time plots at *bottom right* show time course of OIS_{DR} at each site.

background for 40 s at sites 1 and 2 (sites at which the OIS_{DR} was near-maximal). The OIS_{DR} recorded in every slice in which the standard stimulus was delivered to the attached dorsal root ($n = 48$) exhibited similar slow temporal characteristics.

3.2.3 Dorsal horn optical response to local application of K^+ or glutamate

Figure 3.3 shows that a 100-ms pressure-driven application (puff) of either K^+ (15 mM; Fig. 3.3*A*), or glutamate (GLU, 100 μM; Fig. 3.3*B*) to a discrete locus in the DH_s evokes an increase in transmittance that remains confined to the immediate vicinity of the tip of the

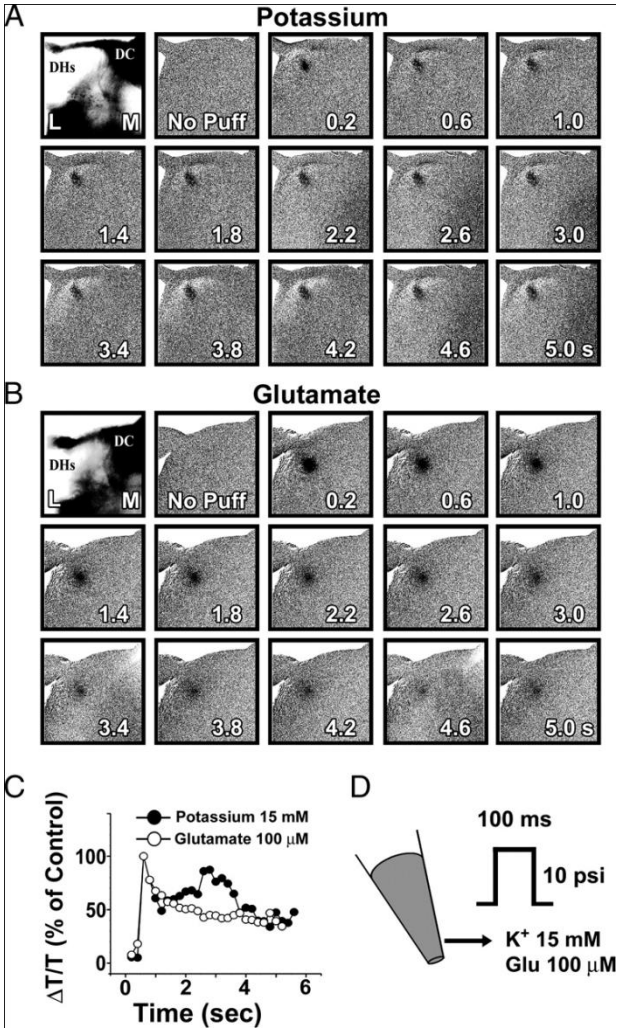

Figure 3.3. Effect of local elevation of $[K^+]_o$ or $[GLU]_o$. Sequence of difference images in *A*: time-course of DH_s optical response to 8 mM K^+ puff (onset at *time 0*). Sequence in *B*: time-course of response to 100 μM GLU puff. *T*/*T* vs. distance plots in *C* show rapid development and persistence of response to K^+ or GLU puff. *D*: puff amplitude, 10 psi; duration, 100 ms.

puffer pipette (dark region in difference image identifies the region of increased transmittance). In the slice that provided the observations in Fig. 3.3, as in the other three slices studied in the same way, the focal increase in transmittance evoked in the DH_s by a 15 mM K^+ puff consistently was smaller in both magnitude and spatial extent than the response evoked at the same site by a 100 μM GLU puff (compare images in Fig. 3.3, *A* and *B*). Despite this considerable difference in magnitude, however, the temporal properties of the

optical response of the DH_s to locally applied K^+ or GLU were similar—i.e., both responses developed relatively rapidly (peaked within 1 s of puff onset) and both declined over an extended time period (15 s; T/T vs. time plots in Fig. 3.3*C* are truncated and thus do not show the total time that the increase in transmittance remained above background).

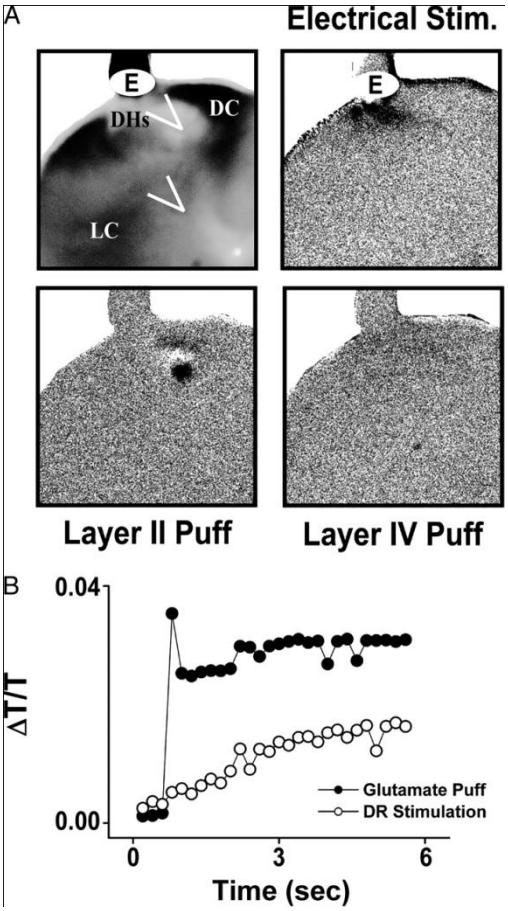

Figure 3.4. Dorsal horn optical responses to electrical stimulation of the dorsal root vs. local (puffer) application of GLU. *A*: reference image at *top left*. Slice orientation as in previous figures. Arrowheads indicate layer II and layer IV sites where tip of puffer pipette made contact with slice. *Top right*: OIS_{DR} evoked by standard dorsal root stimulus (Electrical Stim.). *Bottom*: layer II and layer IV response to GLU puff. ***B*:** time-course of transmittance increase evoked by standard dorsal root stimulus (open symbols) vs. layer II GLU puff (filled symbols).

In the slice that provided the observations in Fig. 3.4*A*, application of a 100 μM GLU puff to layer IV of the dorsal horn evoked an increase in transmittance substantially weaker than that evoked when an identical GLU puff was applied to layer II. A similar result was

obtained in all slices ($n = 6$) in which an identical GLU puff was applied to layer II and to layer IV in the same horn. The T/T versus time plots in Fig. 3.4*B* enable direct comparison of the response evoked by a GLU puff in layer II (plot with ; same slice as in Fig. 3.4*A*) and the OIS_{DR} evoked in the same horn by the standard dorsal root stimulus (plot with). Clearly, the OIS_{DR} not only develops more slowly than the response to the GLU puff, but its magnitude (peak T/T value) is substantially smaller. Similar discrepancies between the responses of the same dorsal horn to GLU puff versus dorsal root stimulation (OIS_{DR}) were observed in every slice ($n = 7$) that we studied in the same way. While direct evidence is lacking, the authors presume that the above-described differences between the OIS_{DR} and the optical response of the DH_s to a GLU puff are due to the temporally and spatially extended, but relatively modest, increase in $[GLU]_o$ associated with the standard dorsal root electrical stimulus versus the abrupt, highly localized, and presumably much larger increase in local $[GLU]_o$ achieved with the GLU puff.

3.3.4 Alterations of the normal relationship between the OIS_{DR} and stimulus-evoked neuroelectrical activity

3.3.4.1 INCREASE OF $[K^+]_O$. Figure 3.5*A* shows the OIS_{DR} (dark regions in difference images) [Figure 4.3.1] recorded before any treatment (control; *top right*), after bath application of ACSF containing 8 mM K^+ (high K^+; *bottom left* in *A*), and after return of the perfusate to normal ACSF containing 3.5 mM K^+ (washout; *bottom right* in *A*). On average (across 3 slices studied in the same way), bath-application of ACSF containing 8 mM K^+ led to a highly significant increase in the magnitude of the OIS_{DR} (to 172.63 ± 4.73% of control; $P < 0.001$). The T/T versus time plots in Fig. 3.5*B* show (for the same slice that provided the

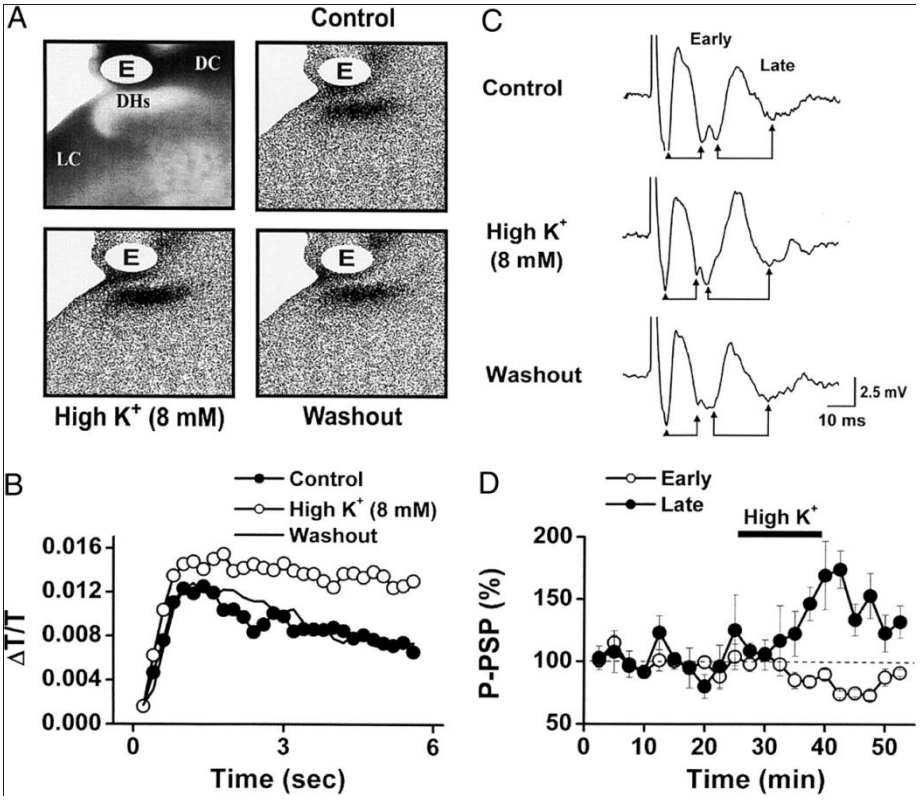

Figure 3.5. Effects of elevated K_o^+. *A*: reference image (*top left*) and OIS_{DR} obtained under control (*top right*), high K^+ (8 mM) (*bottom left*), and washout (*bottom right*) conditions. ***B*:** time-course of OIS_{DR} under each condition. ***C*:** single-pulse, constant-current dorsal root stimulus (P-PSP_{DR}s) recorded under same conditions. Each P-PSP_{DR} average of responses to 10 stimuli; brackets with arrows define early and late components of the P-PSP_{DR}. ***D*:** time-course of effect (average across 5 slices studied in the same way) of 8 mM K^+ on late vs. early components of P-PSP_{DR}. Error bars = ± 1SE.

images in *A*) the detailed time-course of the OIS_{DR} under each condition. After washout of the chamber with ACSF containing normal (3.5 mM) K^+, the magnitude of the OIS_{DR} at most times between 0.0 and 6.0 s after onset of the standard dorsal root stimulus was either the same or very similar to that measured in the same slice before exposure to elevated K^+o. Across the three slices studied in this way, OIS_{DR} magnitude after washout with ACSF containing 3.5 mM K^+ was 102.66 ± 2.77% of control ($P = 0.391$; not significant).

Recordings of the field potential (P-PSP_{DR}) evoked in the DH_s by dorsal root stimulation showed that bath application of ACSF containing 8 mM K^+_o is accompanied by a

progressive increase in the late (long-latency) but not the early component of the response (representative field potentials from an exemplary slice are shown in Fig. 3.5*C*). The results obtained from five slices studied in the same way are summarized in Fig. 3.5*D*. On average, the late component of the P-PSP$_{DR}$ increased progressively in the presence of 8 mM K^+ (plot with), reaching 173.93 ± 12.41% of control at 15 min after onset of the exposure to elevated K^+_o ($P < 0.001$; $n = 5$), whereas the shorter-latency (early) component declined to 75.11 + 3.78% of control (plot with ; $P < 0.001$; $n = 5$ slices). After the solution perfusing the recording chamber was returned to ACSF containing 3.5 mM K^+ (washout), both the early and late components of the P-PSP$_{DR}$ recovered to near-control values.

That the late but not the early component of the P-PSP$_{DR}$ increased in the presence of ACSF containing 8 mM K^+ was observed in each of the five slices. This outcome was not anticipated, but is of some interest because it raises the possibility that an elevation of K^+_o in the DH_s selectively enhances the DH_s response to input conveyed via small-diameter afferents in the dorsal root—i.e., afferents that in intact subjects terminate in peripheral nociceptors and terminate synaptically on neurons in the DH_s, (Hantman et al. 2004; Lu and Perl 2003; Ruscheweyh and Sandkuhler 2001, 2000).

3.3.4.2 INHIBITION OF ASTROCYTE ENERGY METABOLISM. The next experiments sought to evaluate the effects of a selective inhibitor of astrocyte metabolism FAc (Bacci et al. 2002; Hulsmann et al. 2003; Keyser and Pellmar 1994; also see Berg-Johnsen et al. 1993; Watkins et al. 1997) on both and OIS$_{DR}$s were recorded before and after exposure of the slice to ACSF containing 400 μM FAc.

Figure 3.6 shows representative results obtained from one of the four slices studied in this way. The column of color-contoured images at the *left* of Fig. 3.6*A* shows the spatial extent and intensity of the OIS_{DR} recorded before any treatment (control), after onset of bath

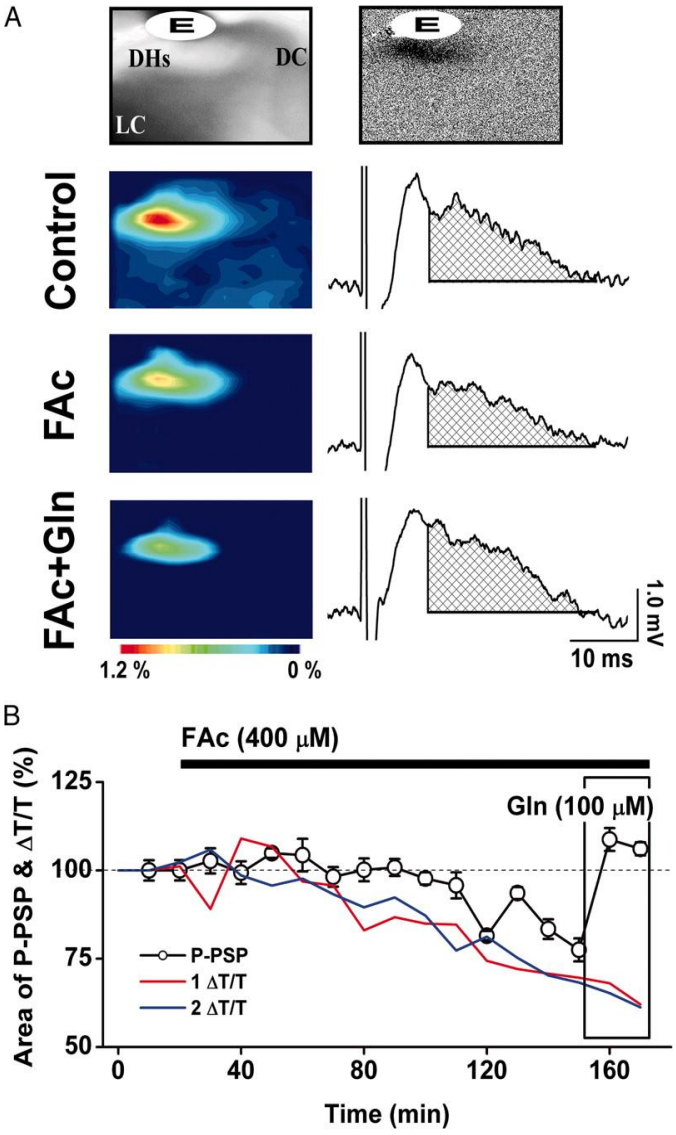

Figure 3.6. Effects of fluoroacetate (FAc; 400 μM) on optical and neuronal responses of the dorsal horn. *A*: reference image at *top left*. *Top right*: OIS_{DR}. *Top* to *bottom* sequence of color-contoured images in *left column*: spatial distribution of OIS_{DR} under control condition (Control), during exposure to bath-applied 400 μM FAc (FAc), and after return to ACSF containing 200 μM glutamine (Gln) + 400 μM FAc (FAc + Gln). *Top* to *bottom* sequence of field potentials in *right column*: P-PSP_{DR} before (Control), during 400 μM FAc (FAc), and after switch of perfusate to ACSF containing 200 μM glutamine + 400 μM FAc. Shaded area in P-PSP_{DR} indicates late component (response between 10 ms after stimulus onset and baseline). Each P-PSP_{DR} average of responses to 10 stimuli. ***B*:** open symbols indicate average across-slice magnitude of the late component of P-PSP_{DR} (5 slices; error bars indicate ± 1SE); solid lines show OIS_{DR} magnitude for 2 slices studied under same conditions. Horizontal bar indicates time of exposure to FAc; rectangle indicates exposure to FAc + Gln.

application of 400 μM FAc, and subsequently, after replacement of the FAc-containing ACSF with ACSF containing FAc + Gln. The P-PSP_{DR}s shown in the column on the *right* of Fig. 3.6*A* were acquired from a different slice than the slice that yielded the optical responses shown at the *left*, were obtained at times and under conditions corresponding to those under which the optical responses were obtained. Visual comparison of the the optical and neuroelectrical responses of the DH_s to dorsal root stimulation. To this end, P-PSP_{DR}s optical and field potential observations in Fig. 3.6*A* shows that both the late component of the P-PSP_{DR} (indicated by shading) and the OIS_{DR} are depressed under FAc. Note that when the perfusate was switched from FAc to FAc + Gln, the magnitude of the late component of the PSP_{DR} recovered to near-normal, but the magnitude of the OIS_{DR} continued to decline to values well below those detected under FAc.

The plots in Fig. 3.6*B* summarize in a more quantitative way the temporal sequence of changes in the magnitude of both the OIS_{DR} and P-PSP_{DR} observed under the above-described FAc and FAc + Gln conditions. Two tendencies are apparent. First, the magnitude of both the OIS_{DR} (average across 5 subjects; open symbols; error bars indicate ± 1SE) and the late component of the P-PSP_{DR} (results from 2 subjects are plotted; solid lines) decline progressively in the presence of ACSF containing 400 μM FAc. Second, after the perfusate was switched to ACSF containing FAc + Gln (last 3 points in plots in Fig. 3.6*B*) the OIS_{DR}

continued to decline, whereas the magnitude of the late component of the P-PSP$_{DR}$ recovered and attained values approaching, if not exceeding, those recorded under control conditions (before exposure to FAc). In other words, the OIS$_{DR}$ and the P-PSP$_{DR}$ became *dissociated* in the presence of FAc + Gln.

3.3.4.3 INHIBITION OF A-TYPE K⁺ CHANNELS. Figure 3.7 shows representative results from a slice in which the OIS$_{DR}$ and the postsynaptic response of the dorsal horn (P-PSP) were measured before and after perfusion of the recording chamber with ACSF containing 100 μM 4-aminopyridine (4-AP). The rationale for evaluating the effects of 4-AP was as follows. If, as the effects of inhibition of astrocyte metabolism (Fig. 3.6) suggest, the OIS$_{DR}$ mainly reflects astrocyte uptake of K^+ and/or GLU, interference with outward K^+ transport in both astrocytes and neurons via A-type K^+ channels also should alter the OIS$_{DR}$ and P-PSP$_{DR}$ in opposite ways. More specifically, if the OIS$_{DR}$ mainly reflects astrocyte clearance of K^+ and GLU, 4-AP should decrease the OIS$_{DR}$ (due to 4-AP block of astrocyte K^+ uptake) but increase the P-PSP$_{DR}$ (because of the increase in neuronal excitability due to the block by 4-AP of outward K^+ currents in both pre- and postsynaptic neurons).

As predicted, the optical and neuronal responses of the dorsal horn evoked by electrical stimulation of the dorsal root dissociated in the presence of 4-AP. More specifically, both the early and late components of the P-PSP$_{DR}$ increased under 4-AP (the late component exhibited the largest increase; plots in Fig. 3.7*D*; see also Fig. 3.7*B*), whereas the OIS$_{DR}$ decreased (compare control and 4-AP images in Fig. 3.7*A*). Similar results were obtained in all four slices studied in the same way. On average, the early and late components of the P-PSP increased by 151.63 ± 5.41% ($P < 0.001$; $n = 4$) and 318.09 ± 50.66% ($P < 0.001$, $n = 4$), respectively, whereas the OIS$_{DR}$ decreased to 26.19% ±4.32% of control ($P < 0.001$, $n = 4$).

Other experiments detected a dissociation of the dorsal horn optical and neuronal responses to dorsal root stimulation when the ACSF contained 5 mM cesium chloride (CsCl; data not shown)—CsCl was studied because it has been shown (Janigro et al. 1997) to block inwardly rectifying (K_{IR}) potassium channels widely presumed to contribute to astrocyte-mediated K^+_o homeostasis (Kofuji and Newman 2004; Newman 2004; Olsen and Sontheimer 2004; Simard and Nedergaard 2004; Walz 2000).

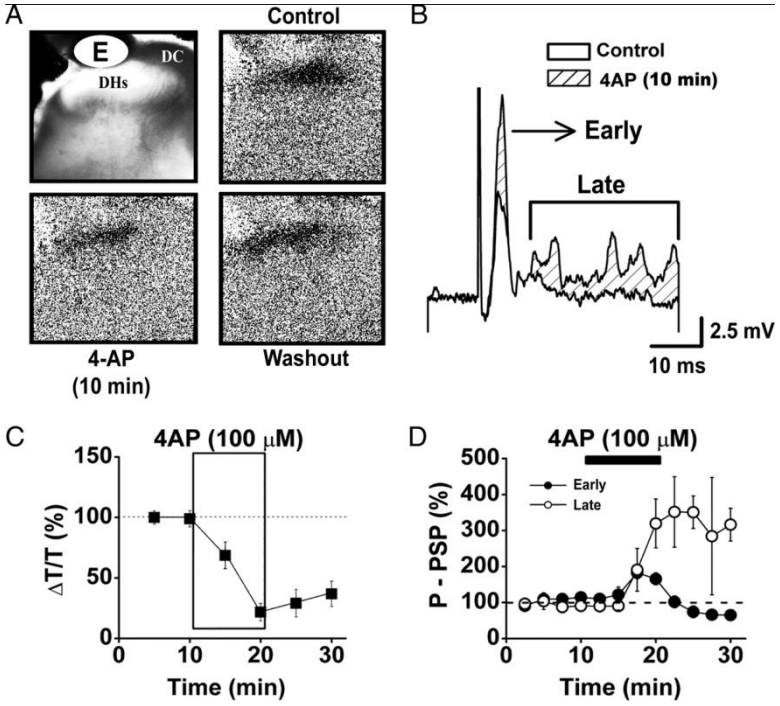

Figure 3.7. Effects of 4-aminopyridine (4-AP) on OIS_{DR} and P-PSP_{DR}. ***A*:** reference image at *top left*. *Top right*: OIS_{DR} before treatment (Control). *Bottom left*: OIS_{DR} after 100 μM 4-AP. *Bottom right*: OIS_{DR} after return to drug-free ACSF (Washout). ***B*:** P-PSP_{DR}s under control and 100 μM 4-AP conditions. ***C*:** *T*/*T* vs. time plot showing that OIS_{DR} decreased after 4-AP (exposure to 4-AP indicated by rectangle). ***D*:** effect of 4-AP on early () and late () components of P-PSP_{DR}.

3.3.5 Studies of slices from formalin-injected animals

3.3.5.1 OIS_{DR} AFTER INTRACUTANEOUS FORMALIN INJECTION. The pair of images on the *right* in Fig. 3.8 (Formalin) were obtained from the horn on the same side as the hindpaw that received an intracutaneous injection of 25 μl of 5% formalin 4 days before the

experiment. In contrast, the image pair on the left (Fig. 3.8; Control) were obtained from the opposite horn in the same slice. The difference images at the *bottom* of Fig. 3.8 show the OIS_{DR} evoked in each horn by the standard dorsal root stimulus. Note that the OIS_{DR} recorded from the horn on the same side of the formalin injection (*bottom right*) is extremely small, whereas on the opposite side of the same slice (*bottom* similar result was obtained in each of the 10 slices from subjects that received an intracutaneous injection of formalin 3–5 days before the experiment. On average, the OIS_{DR} evoked by the standard dorsal root stimulus in the horn ipsilateral to the formalin injection site was only 37.19 ± 5.92% ($P < .001$; $n = 10$) of the control OIS_{DR} recorded from the DH_s on the side contralateral to the injection.

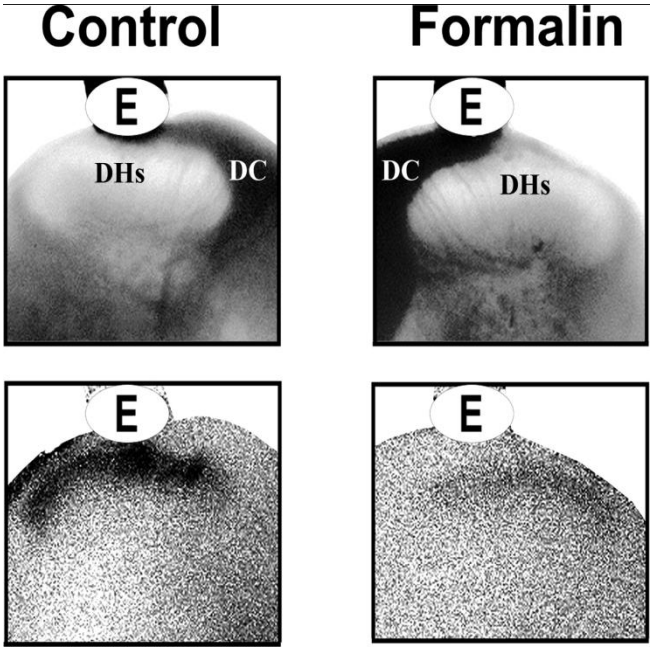

Figure 3.8. Intracutaneous formalin injection attenuates the OIS_{DR} in the ipsilateral dorsal horn. *Top row*: reference images from same slice showing horns contralateral (Control; *left*) and ipsilateral (Formalin; *right*) to formalin injection site. *Bottom row*: OIS_{DR} recorded contralateral (*left*) and ipsilateral (*right*) to injection site.

In four subjects, the rostrocaudal extent of the attenuating effect of an intracutaneous injection of 5% formalin on the dorsal horn was determined by recording the OIS_{DR} not only

from the ipsilateral (on the same side as the formalin injection site) and contralateral horns at the level of the cord at which most afferents from the injected skin site (volar hindpaw) enter the spinal cord (segmental level L_4) (Takahashi and Nakajima 1996; Takahashi et al. 2002), but also from both horns *left*), the magnitude of the OIS_{DR} is typical of that recorded in the DH_s of an untreated subject. A of slices cut from successively more rostral levels of the same spinal cord (i.e., at 0.8, 1.6, 2.4, 3.2, and 4.0 mm rostral to level 0; slice thickness was 400 μm). In three of the spinal cords studied in this way, the most rostral level studied (level 4.0) was L_1; in the remaining subject it was L_2.

At level L_4, the magnitude of the OIS_{DR} recorded from the DH_s on the same side as the formalin injection was only 51.5 ± 6.2% ($P < .001$; $n = 4$ slices) of the OIS_{DR} recorded in the contralateral horn, and this discrepancy remained essentially undiminished for 1.6 mm rostral to L_4. At levels 2.4 mm rostral to L_4, however, no effect of the intracutaneous formalin injection on the OIS_{DR} evoked in the ipsilateral DH_s was evident—i.e., at distances 2.4 mm above the level (L_4) at which most afferents from the hindpaw injection site enter the spinal cord, the average magnitude of the OIS_{DR} evoked in the ipsilateral DH_s by the standard stimulus did not differ significantly from the average magnitude of the OIS_{DR} recorded in the DH_s on the opposite side (i.e., at levels >2.4 mm rostral to L_4, the OIS_{DR} recorded in the ipsilateral DH_s was 89.43% of the OIS_{DR} recorded in the contralateral DH_s ($P > 0.04$; $n = 6$ slices; not significant).

3.3.5.2 INTRACUTANEOUS FORMALIN INJECTION REDUCES THE NORMAL IMPACT OF ELEVATED $[K^+]_O$ ON THE OIS_{DR}. When $[K^+]$ in the ACSF was 3 mM (control), the time-course of the OIS_{DR} evoked in the DH_s on the same side as the formalin injection site (ipsilateral; the formalin side) and in the DH_s on the opposite side (contralateral; the normal

side) are very similar (compare normalized T/T vs. time plots with filled symbols in Fig. 3.9, *A* and *B*). More specifically, regardless of whether the horn receives afferent input from an untreated skin site or from a formalin-injected skin site (the T/T values of all the plots in Fig. 3.9, *A* and *B*, are normalized; i.e., expressed in terms of percent of the maximal value recorded under each condition), the transmittance increase evoked in the DH_s by stimulation of the dorsal root peaks at about 10 s after stimulus onset, and over the next 30–60 s declines toward baseline.

In contrast, when the ACSF bathing the slice is elevated (contains 8 mM K^+), the temporal profile of the transmittance increase evoked in the dorsal horn contralateral (the normal side) to a formalin-injected skin site is very different from the transmittance increase evoked in the horn ipsilateral (the formalin side) to the injection site (compare normalized T/T vs. time plots with open symbols in Fig. 3.9, *A* and *B*). As described previously (e.g., Fig. 3.5), in the presence of ACSF containing 8 mM K^+, the increase in transmittance evoked by dorsal root stimulation in the DH_s on the side contralateral to the formalin injection not only did not return to baseline during the 50 s period during which it was sampled (unlike the response of the same horn to the same dorsal root stimulus when $[K^+]$ in the ACSF was 3 mM), but the increase in transmittance remained near maximal over the entire period (60 s) during which images were acquired. Clearly, therefore the duration of the transmittance change evoked in the DH_s contralateral to the formalin injection (the normal side) is substantially prolonged when $[K^+]_o$ is 8 mM, whereas in the DH_s on the same side as the formalin injection (the formalin side), the duration of the transmittance change evoked by the standard dorsal root stimulus modifies only slightly in the presence of elevated K^+_o.

3.3.5.3 INTRACUTANEOUS FORMALIN INJECTION REDUCES THE DORSAL HORN OPTICAL RESPONSE TO LOCAL APPLICATION OF GLU. A final series of slices ($n = 3$) was studied to determine the effects of formalin on the optical response of the lumbosacral dorsal horn to puffer application of 100 μM GLU. The difference images in Fig. 3.9*C* are

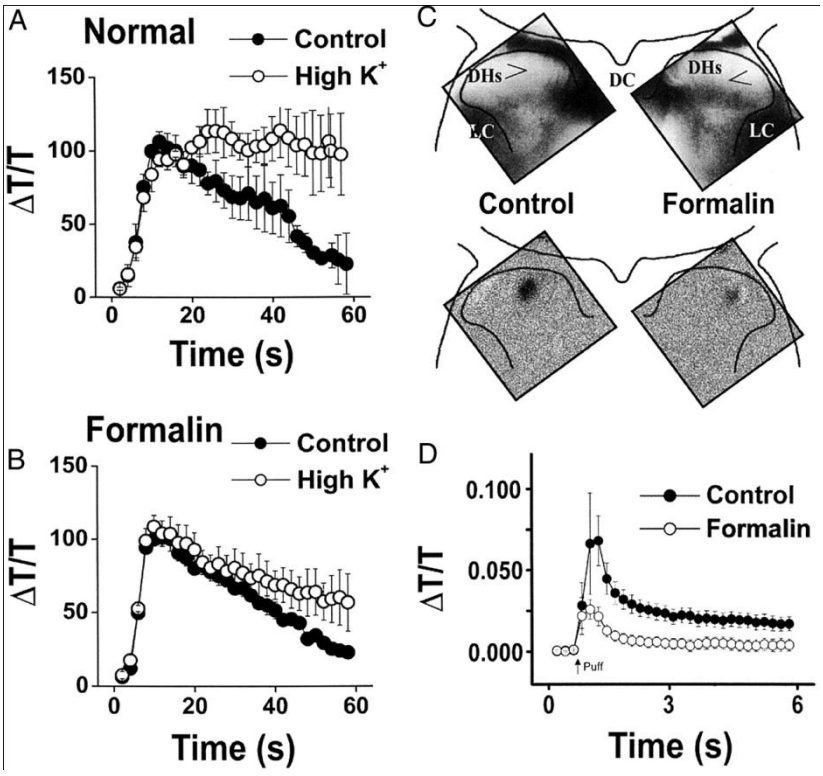

Figure 3.9. Formalin injection attenuates effect of elevated K^+_o on the OIS_{DR} and suppresses the response to puffer-applied glutamate. ***A*** **and** ***B***: *T*/*T* vs. time plots for horn contralateral (Normal/Control) and ipsilateral (Formalin) to formalin-injected skin site. Filled symbols indicate average (across 3 horns studied in the same way) transmittance increase evoked by standard dorsal root stimulus under control condition. Open symbols indicate average transmittance increase during perfusion with ACSF containing 8 mM K^+. Error bars indicate ± 1SE. ***C***: reference (*top row*) and difference images (*bottom row*) showing response to puffer-applied GLU on both control and formalin sides of same slice. ***D***: *T*/*T* vs. time plots showing magnitude and time course of optical response (average across 3 slices) of control vs. formalin horns to puffer-applied 100 μM Glu. Error bars indicate ± 1SE.

representative and reveal that 4 days after intracutaneous formalin injection (volar hindpaw), a GLU puff evokes a prominent local increase in transmittance in the lumbosacral dorsal horn on the side opposite to the skin site that received the injection (dark region in control image), but an identical puff evokes a much smaller transmittance increase in the DH_s on the same

side as the skin site injected with formalin (formalin image). The T/T versus time plots in Fig. 3.9*D* summarize, for the same slice shown in Fig. 3.9*C*, the time-course of the transmittance increase on the control versus formalin sides evoked by a 100-ms puff of 100 μM GLU. For the three slices studied in this way, the average (across-subject) DH_s response to direct GLU application on the side of the formalin injection was only 32.6 ± 5.2% ($P < 0.001$) of the DH_s response evoked by an identical puff on the control side.

3.4 DISCUSSION

3.4.1 Dorsal horn optical response—origins and underlying mechanisms

The findings obtained in the initial experiments (Figs. 3.1 and 3.2) show that, although the OIS_{DR} depends on synaptic neurotransmission, its slow development and prolonged persistence are uncharacteristic of stimulus-evoked neuronal activity. This alerted us to the possibility—one already proposed by others (Asai et al. 2002)—that the OIS_{DR} may be nonneuronal in origin. Subsequent experiments showed (Figs. 3.3 and 3.4) that the optical response of the dorsal horn to a 100-ms local application of K^+ or GLU is very prolonged, leading us to consider that it, like the OIS_{DR}, primarily reflects nonneuronal mechanisms/processes.

Although direct evidence is lacking, a wealth of published observations is consistent with the possibility that astrocytes are the major source of the transmittance increase that underlies both the OIS_{DR} and the dorsal horn optical response to puffer-applied K^+ or GLU. For example, astrocytes in the dorsal horn and other CNS regions undergo morphological/biophysical modifications (e.g., cell volume increases, light scattering decreases) that are closely coupled to stimulus-evoked increases in excitatory afferent drive.

Furthermore, astrocyte-mediated clearance of the excesses in extracellular K^+ and/or GLU that accompany increased postsynaptic neuronal activity is accompanied by prominent and prolonged alterations of cell volume and tissue light scattering. In addition, astrocyte uptake of GLU_o and K^+_o is metabolism-dependent and occurs via astrocyte-specific membrane transporters (Huang et al. 2004; Kawahara et al. 2002; Rosenberg et al. 1992) and carrier- and channel-operated potassium chloride uptake (Walz 2000), respectively.

The unusual temporal characteristics of the optical response of the DH_s to a 100-ms puff of 15 mM K^+ (i.e., rapid onset, decay, followed by a secondary increase) reinforce the suggestion that the response is, in the main, attributable to astrocytes. For example, the rapid initial increase in transmittance seems explicable in terms of an initially rapid uptake of excess K^+_o by astrocytes in the vicinity of the puffer pipette (K^+ uptake is accompanied by obligatory uptake of water and astrocyte swelling; Sykova et al. 2003), whereas such a secondary (delayed) increase in transmittance is expected if local transient neuronal excitation was evoked by the K^+ puff. That is, puff-evoked neuronal excitation not only would be accompanied by a local release of GLU from presynaptic nerve terminals but, after a delay, by astrocyte re-uptake (along with water) of the released GLU, and a renewed (delayed) phase of astrocyte swelling. Another possibility is that the secondary, delayed increase in DH_s transmittance that follows a 15 mM K^+ puff reflects astrocyte uptake of K^+-evoked GLU release from astrocytes (Volterra and Bezzi 2002).

A second example of an aspect of the dorsal horn optical response to puffer-applied K^+ or GLU that fits with the idea that the response is astrocytic in origin is that the response of lamina II to puffer-applied K+ or GLU consistently is larger in spatial extent and magnitude than the response evoked by application of an identical puff to lamina IV (e.g., Fig.

3.4). This observation is in accord with the report (Svoboda et al. 1988) that, in normal subjects, $[K^+]_o$ is maintained at lower values in the superficial dorsal horn (laminae I–II) than in the deeper laminae (laminae III–V) and raises the possibility that the capacity of laminae I–II astocytes to take up K^+ and GLU (along with water) may be greater than that of layer IV astrocytes. Interestingly, a differential capacity of astrocytes in the superficial versus deep dorsal horn to take up K^+ and GLU would be compatible with recent demonstrations that K^+ channels and aquaporins tend to colocalize in astrocyte membranes, and aquaporin expression is higher in the superficial dorsal horn than in the deeper laminae (Asai et al. 2002; see also Binder et al. 2004).

If the OIS_{DR} is, in fact, attributable to light scattering changes that accompany astrocyte uptake of K^+ and GLU, it should be possible to dissociate the dorsal horn optical and neuronal responses evoked by stimulation of the dorsal root. Two series of experiments were carried out to address this possibility. The first evaluated the effects on the optical (OIS_{DR}) versus neuronal ($P\text{-}PSP_{DR}$) responses to dorsal root stimulation of selective inhibition of astrocyte metabolism with bath-applied FAc (400 μM). The second experiments of this type evaluated the effects of bath-applied 4-AP, an agent that blocks A-type (rapidly inactivating) membrane potassium channels in both astrocytes and neurons.

3.4.1.1 EFFECTS OF FAC. The following information about the cellular actions of FAc is essential for full appreciation of the results: *1*) FAc inhibits the enzyme aconitase in the Krebs cycle of astrocytes, but does not affect neuronal metabolism-linked energy production (Clarke et al. 1970; Hassel et al. 1992, 1997; Hulsmann et al. 2003; Keyser and Pellmar 1994; Muir et al. 1986; Paulsen et al. 1987; Waniewski and Martin 1998); *2*) FAc blocks both astrocyte production and release of glutamine (Gln) and thus reduces the availability of

extracellular Gln for uptake by the presynaptic terminals of glutamatergic dorsal root afferents (Bacci et al. 2002); *3*) glutaminergic neurotransmission fails in the presence of FAc due to decline of adequate GLU in the presynaptic terminals of dorsal root afferents (Bacci et al. 2002), but this decline can be avoided if an adequate supply of extracellular Gln is provided; and *4*) provision of an adequate level of Gln_o enables replenishment of the GLU in nerve terminals even in the continuing presence of FAc (because FAc does not affect the capacity of nerve terminals to take up and convert Gln to GLU), and enables complete recovery of glutaminergic neurotransmission even though FAc continues to inhibit astrocyte energy metabolism (Bacci et al. 2002).

The observations obtained after inhibition of astrocyte metabolism with FAc (Fig. 3.6) can be interpreted as follows. First, the declines in the magnitude of both the OIS_{DR} and the $P\text{-}PSP_{DR}$ (especially the late component of the $P\text{-}PSP_{DR}$) that occurred during the exposure to FAc reflect, respectively, inhibition of astrocyte metabolism by FAc (because of the FAc-induced reduction of energy-dependent astrocyte uptake of K^+ and GLU), and a disappearance of GLU in the presynaptic terminals of dorsal root afferents (due to FAc inhibition of astrocyte Gln production and release, which in turn, reduces the $[Gln]_o$ available for uptake by the presynaptic terminals of glutaminergic dorsal root afferents). Second, the dissociation of the dorsal horn optical and neurophysiological responses after switch of the bath to FAc + Gln (plots at *bottom* of Fig. 3.6; the $P\text{-}PSP_{DR}$ returns to control levels, whereas the OIS_{DR} continues to decline) reflects restoration of stimulus-evoked dorsal horn glutaminergic neurotransmission due to restoration of $[Glu]_i$ in presynaptic nerve terminals (i.e., by the Gln provided in the ACSF that bathed the slice). The OIS_{DR} continued to decline

in the presence of FAc + Gln because of the continuing FAc-mediated inhibition of astrocyte metabolism.

3.4.1.2. EFFECTS OF 4-AP. Although the specific functional role(s) of rapidly inactivating A-type K^+ currents in astrocytes remain(s) to be established, outward K^+ currents are known to contribute to astrocyte-mediated spatial buffering and siphoning of K^+ (Bekar and Walz 2002). With this in mind, the *a priori* prediction was that block of A-type K^+ channels with 4-AP would antagonize K^+ uptake by astrocytes (and thus reduce or eliminate the OIS_{DR}), and at the same time enhance stimulus-evoked dorsal horn neurotransmission (and thus increase the magnitude of the P-PSP_{DR} evoked by dorsal root stimulation) due to the increased excitatory neurotransmitter release expected to accompany block of A-type K^+ currents in the presynaptic terminals of dorsal root afferents. We therefore expected dissociation of the OIS_{DR} and the postsynaptic response of dorsal horn neurons to dorsal root stimulation (P-PSP_{DR}) under 4-AP. The results shown in Fig. 3.7 are viewed as fully consistent with this prediction.

3.4.2 Dorsal horn astrocytes after intracutaneous injection of formalin

Experiments on slices from subjects that had received an intracutaneous injection of 5% formalin to the volar hindpaw 3–5 days before the experiment revealed that, in the horn on the same side (ipsilateral) as the injected skin site, the optical responses evoked by electrical stimulation of the dorsal root (Fig. 3.8) and also by direct application of K^+ or GLU (Fig. 3.9) were substantially smaller than those recorded in the opposite horn (relative to the responses evoked in the contralateral dorsal horn). This outcome is interpreted to indicate that astrocytes in the dorsal horn on the same side of the formalin injection are relatively

unresponsive to an elevation of $[K^+]_o$ or [GLU]. Furthermore, in contrast to the marked prolongation of the time-course of the OIS_{DR} that occurs in an untreated subject during an exposure to elevated K^+_o (to 8 mM), the same elevation of K^+_o had little or no impact on the time course of the OIS_{DR} recorded in the lumbosacral horn on the same side as the hindpaw injected with formalin (Fig. 3.9, *A* and *B*). This insensitivity of the OIS_{DR} on the same side as the formalin-injected skin site to elevated K^+_o or GLU strongly suggests that astrocytes in the region of the dorsal horn that receives its afferent input from the formalin-injected skin region are unable to clear the extracellular compartment of excess K^+ and GLU and do not take up water and swell (and thus tissue light scattering does not alter) in response to the increases in K^+_o and GLU_o that accompany increased dorsal horn neuroelectrical activity. As a consequence, K^+_o and GLU_o (and thus neuronal excitability) in the DH_s remain elevated for an abnormally prolonged period following stimulus-evoked dorsal horn neuronal activity.

3.4.3 Contributions of impaired astrocyte homeostatic function to the abnormal dorsal horn neuron properties that develop after intracutaneous formalin injection

Although it is recognized that perisynaptic astrocytes normally function as active partners in normal CNS synaptic neurotransmission (Newman 2004), the results of this study suggest that, under a variety of pathological conditions (i.e., inflammation, injury, infection), astrocytes are unable to function as fully active partners in CNS neurotransmission. The finding (Coull et al. 2003) that peripheral nerve injury is accompanied by trans-synaptic reduction in the expression of the potassium-chloride exporter KCC2 in dorsal horn lamina I neurons—an alteration that disrupts lamina I neuron anion homeostasis—seems highly

relevant to altered dorsal horn glia–neuron interactions and their potential contributions to hyperalgesia/persistent pain.

Coull et al. (2003) showed that the nerve injury-induced decrease in the expression of KCC2 identified by results in the intracellular accumulation of Cl^- in lamina I neurons, resulting in a shift of the equilibrium potential for Cl^- that causes $GABA_A$ receptor mediated synaptic currents (normally hyperpolarizing) to become depolarizing (excitatory). As a result, affected neurons in lamina I (and, presumably, also in the other layers of the DH_s) exhibit increased excitability, acquire spontaneous activity, and develop abnormal responsivity to nonnoxious environmental stimulation that may account, at least in part, for the hyperalgesia/persistent pain detected by behavioral assays of nerve-injured subjects.

Because the decrease in lamina I neuron KCC2 expression occurs relatively late after nerve injury (15–17 days; Coull et al. 2003), it unlikely is a direct result of the injury. Instead, it may be the lamina I neuron response to a maintained increase in superficial dorsal horn $[K^+]_o$ and $[GLU]_o$ that accompanies the prominent dorsal horn glial activation associated with peripheral nerve injury (e.g., Milligan et al. 2001). In addition, if the demonstration (Kaila et al. 1997; using hippocampal pyramidal neurons; also Payne et al. 2003) that even a brief (seconds) exposure to a modest elevation of K^+_o (to 8 mM) induces increases in neuronal $[Cl^-]_i$ that account for a +16- to +18-mV shift in E_{GABAA} applies to dorsal horn neurons, an impaired ability of astrocytes to buffer $[K^+]_o$ and $[GLU]_o$ following intracutaneous formalin injection might not only lead to abnormally prolonged elevations of neuronal excitability due to excess K^+_o and GLU_o, but also to neuronal abnormalities characterized by a loss of GABA-mediated inhibition and hyperalgesia/persistent pain.

Chapter 4

Effects of alteration of glia on neuronal activity

4.1 Background

Direct application to the spinal cord of a variety of substances (e.g., excitatory neurotransmitters such as substance P or NMDA receptor agonists) or low-frequency nociceptor afferent input can produce a long-term enhancement of excitatory synaptic transmission between C-fibre afferents and neurons in the DH_s (Ikeda et al. 2006; Sandkuhler, 2000; Liu and Sandkuhler, 1998). Clearly, therefore, establishment of the long-term enhancement of DH_s excitatory synaptic transmission that underlies central sensitization, secondary hyperalgesia, and persistent pain does not, as previously believed, require a sustained preceding period of high-frequency nociceptor afferent activation.

The experiments described in this paper were motivated by the intriguing and clinically relevant possibility that a long-term enhancement of DH_s excitatory synaptic transmission not only can occur in the absence of a preceding period of conditioning afferent drive (as described above), but also can arise subsequent to an impairment of DH_s glial energy metabolism. Observations reported in previous studies are fully consistent with the idea that impairment of the ability of astrocytes to regulate extracellular K^+ and glutamate levels alters excitatory neurotransmission at multiple levels of the CNS. As examples: (1) the secondary hyperalgesia that follows intradermal injection of 5% formalin is accompanied by an impaired ability of astrocytes to regulate $[K^+]_o$ and $[glutamate]_o$ in the region of the DH_s

that receives its input from the injected skin site (Lee et al. 2005; Svoboda et al. 1988), (2) even a brief (40 sec) increase in extracellular K^+ induces LTP in the hippocampal slice (Fleck et al. 1992); (3) hippocampal LTP is substantially reduced in animals in which astrocytes are rendered unable (via a selective genetic manipulation) to release neurotransmitters (Pascual et al. 2005); (4) d-serine released from astrocytes is critical for the induction of LTP in hippocampal slices (Yang et al. 2003); (4) the slow astrocytic depolarization that accompanies hippocampal LTP is due to astrocyte uptake of K^+ and supports neuronal LTP by reducing the efficacy of astrocytic glutamate transporters and inducing astrocyte release of a variety of signaling molecules (for review see Ge and Duan, 2006); and, finally, (5) intracerebral injection of fluorocitrate (a reversible, selective inhibitor of glial metabolism, Fonnum et al. 1997; Paulsen et al. 1987) elevates $[K^+]_o$, increases cortical neuron excitability, and induces focal epileptiform discharge (Willoughby et al. 2003).

The goals of this study were to: (1) investigate the possibility that transient impairment of spinal cord glial energy metabolism can, in the absence of a preceding period of conditioning afferent drive, initiate the long-term enhancement of DH_s excitatory synaptic transmission widely regarded to underlie central sensitization, secondary hyperalgesia, and persistent pain (Sandkuhler, 2000; Watkins and Maier, 2002); and, (2) acquire information bearing directly on the validity of the recent proposal that impaired astrocytic regulation of $[K^+]_o$ can lead to conversion of the effect of GABA on DH_s neurons from inhibition to excitation (Lee et al. 2005; Garcia-Nicas et al. 2006; Coull et al. 2003).

4.2 Results

4.2.1 Population-level observations -

4.2.1.1. effects of FC on the OIS_{DR} – In each of 3 slices the OIS_{DR} evoked in the ipsilateral DH_s by electrical stimulation of the dorsal root was recorded at regular intervals (i) before ("Control"), (ii) throughout a 20 min exposure to ACSF containing 50 μM FC ("FC"), and (iii) during the 60 min period following the restoration of perfusion with drug-free ACSF ("Washout"). Labels in the top left image in Figure 4.1A (grayscale) identify the position of the DH_s, the location of the tip of the stimulating electrode (E - in the part of the dorsal root entry zone that overlies the medial half of the DH_s), and the structures which border the DH_s on the left side of the slice (e.g., DC - dorsal column; LC - lateral column; VH - ventral horn). The colour-coded average difference images in Figure 4.1A (i.e., average prestimulus – poststimulus images) show that not only did the OIS_{DR} decrease in both intensity (ΔT/T) and spatial extent during the 20min exposure to 50 μM FC (FC *vs.* Control images), but it continued to decrease during the 60 min period after the perfusion solution was returned to drug-free ACSF (FC *vs.* Washout images). The across-slice (n = 3) plot of mean ΔT/T *vs.* time in Figure 4.1B shows the time course of the effect of FC on the OIS_{DR} (filled circles).

4.2.1.2. effects of FC on the $P\text{-}PSP_{DR}$ – The superimposed field potential recordings (each trace is the average response to 10 stimulus trials) in Figure 4.1C illustrate the effect of FC on the population postsynaptic potential ($P\text{-}PSP_{DR}$) evoked in the ipsilateral DH_s by a single-pulse constant-current stimulus to the attached dorsal root. Note that although for this exemplary slice the $P\text{-}PSP_{DR}$ recorded during the exposure to FC (orange trace - FC) is slightly smaller than the potential recorded prior to the exposure to FC (black trace – Control), the $P\text{-}PSP_{DR}$ recorded after restoration of the perfusion solution to drug-free normal ACSF (red trace – Washout) is substantially larger than the $P\text{-}PSP_{DR}$ recorded prior to the exposure to FC.

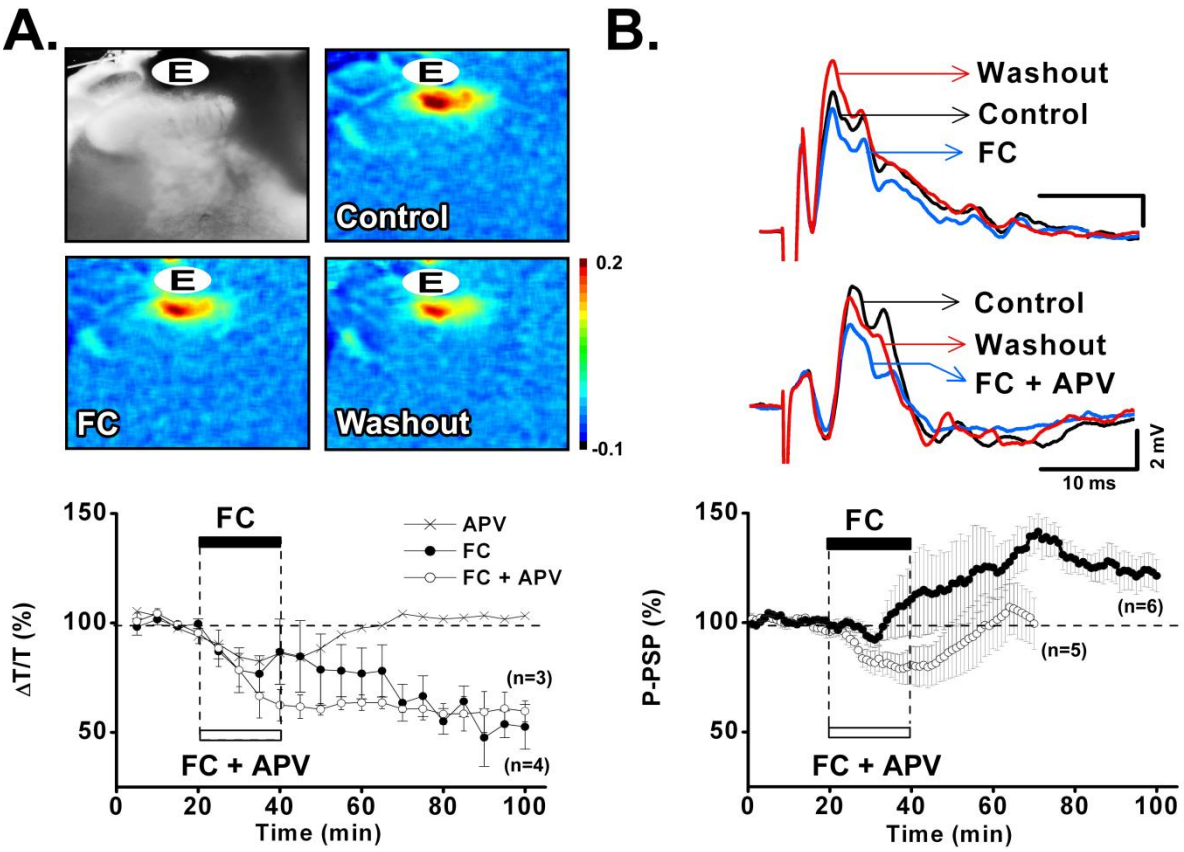

Figure 4.1. FC modification of the optical and neuronal responses of the DH_s. A: Effect of FC on the optical intrinsic signal (OIS_{DR}). Reference image (grayscale) showing location of stimulating electrode (E) and anatomical regions within the image field – superficial dorsal horn (DH_s); dorsal column (DC); ventral horn (VH); and lateral column (LC). Colour scale at right indicates OIS_{DR} intensity ($\Delta T/T \times 100$) and applies to each average difference (prestimulus – poststimulus) image (Control, FC, and Washout). B: Time course of effect on OIS_{DR} of 50 µM FC (filled circles), 50 µM FC + 50 µM APV (open circles), and 50 µM APV (gray squares). C: Average across-trial field potential (average P-PSP_{DR} to 10 stimuli) recorded from DH_s during control, exposure to FC, and washout periods. D: Time course of effect on P-PSP_{DR} of 50 µM FC (filled circles) *vs.* 50 µM FC + 50 µM APV (open circles). Each point indicates amplitude of potential averaged across ten consecutive trials. Horizontal bars in B and D identify 20 min period slice was exposed to each treatment; error bars = ±1SE.

Figure 4.1D shows the average across-slice (n=6) time course of the effect of FC on the P-PSP_{DR} (plot with filled circles). In each of 6 slices studied in this way exposure to FC was followed (during the initial 20-35min of the 60min washout period) by a substantial increase in P-PSP_{DR} amplitude (the peak increase in the P-PSP_{DR} during washout ranged between 140-168%; mean = 153%; n = 6). Over the last 30 – 35 min of the washout period P-

PSP_{DR} magnitude declined progressively, but in no slice did P-PSP_{DR} amplitude return to values measured prior to FC exposure (P-PSP_{DR} amplitude at the end of the 60 min washout period was 115-132% of Control; mean = 124%; n = 6).

Similar to the findings reported in previous studies of the long-term effects of repetitive afferent drive on glutaminergic neurotransmission at a variety of sites in the CNS (e.g., spinal cord dorsal horn – Sandkuhler, 2000; hippocampus –Bliss and Collingridge, 1993; Malenka, 1994; Linden, 1999; neocortex –Rioult-Pedotti et al. 2000; Artola and Singer, 1987), LTP_{FC} apparently requires NMDA receptor activation because no facilitation of DH_s excitatory neurotransmission occurred when APV (at a concentration that achieves a nealy complete block of NMDA receptors; 50 μM; plot with open circles at Figure 4.1D; n = 5) was present in the perfusion solution during the time the slice was exposed to FC. In contrast, FC's suppression of the OIS_{DR} apparently does not require NMDA receptor activation because exposure to APV + FC (plot with open circles at Figure 4.1B) failed to significantly alter either the magnitude or time course of the reduction of the OIS_{DR} that followed exposure to FC. Consistent with the demonstration that magnitude of the OIS_{DR} depends on glutamatergic neurotransmission (Murase et al. 1998; also Lee et al. 2005), APV application alone led to a modest suppression of the OIS_{DR} (plot with gray squares at Figure 4.2B) that reversed and returned to control levels 20-25 min after the perfusion solution was restored to drug-free, normal ACSF.

The possibility that excess local accumulation of K^+ in the DH_s might, at least in part, be responsible for FC's long-term alteration of DH_s excitatory neurotransmission was evaluated by varying (from one slice to the next) the $[K^+]_o$ in the perfusion solution during

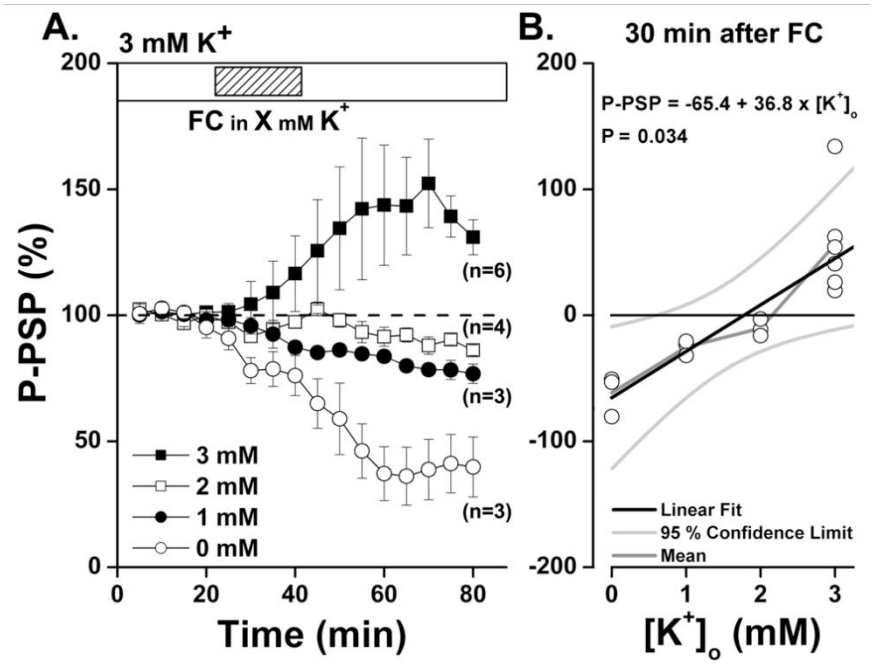

Figure 4.2. Dependency on K^+_o of FC-induced modification of DH_s neurotransmission. A: Plots showing that effect of FC on the $P\text{-}PSP_{DR}$ alters systematically as $[K^+]_o$ is varied over the range 0-3 mM. Format same as Figure 1B. B: Linear regression analysis of the relationship between magnitude of FC-induced alteration of $P\text{-}PSP_{DR}$ and $[K^+]_o$ revealing that over the range 0-3 mM a 1 mM change of $[K^+]_o$ is accompanied by nearly a 37% alteration of DH_s neuron responsivity. Note that at $[K^+]_o$ values less than 1.8 mM FC induces LTD; however, at values exceeding 1.8 mM FC induces LTP.

the exposure to FC. The plots of $P\text{-}PSP_{DR}$ magnitude *vs.* time in Figure 4.2A show that the effect of the exposure to FC modified strikingly and systematically as $[K^+]_o$ in the perfusion solution (and, therefore, in the DH_s) was varied over the range 3.0 – 0.0 mM. Reduction of K^+ in the ACSF by 1 mM (i.e., to 2 mM; plot with open squares in Figure 4.2A) eliminated the long-term enhancement of DH_s neurotransmission detected when FC was provided to the slice in normal ACSF. Moreover, when $[K^+]$ in the perfusate was 1mM or less, exposure to FC was followed by a long-term depression of the $P\text{-}PSP_{DR}$ (LTD_{FC}; plots with filled and open circles). Statistical analysis of the data obtained from each slice and under each condition at 30 min after exposure to FC revealed that the $[K^+]_o$ dependency of FC's effect on the magnitude of the DH_s response to small-diameter afferent drive is linear and

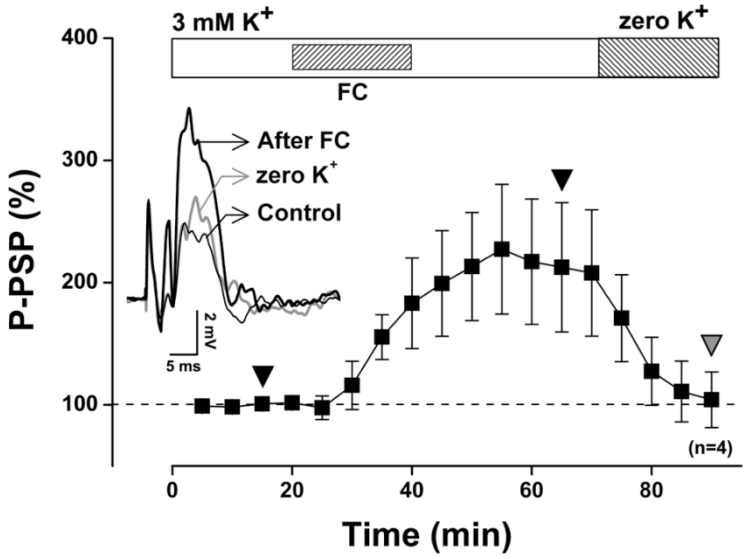

Figure 4.3. Lowering $[K^+]_o$ eliminates the LTP that follows exposure to FC. Inset - superimposed average DH_s field potentials ($P\text{-}PSP_{DRs}$; each trace shows the average response to 10 stimuli) recorded from same DH_s site during the control period (at 15 min after the start of recording), and at 60 and 90 min (indicated by arrowheads), respectively. Shaded regions in horizontal bar at top indicate exposures to FC and zero K^+; slice was exposed to ACSF containing 3 mM K^+ during initial 70 min of the study.

statistically significant (Figure 4.2B; $p = 0.034$; $P\text{-}PSP_{DR} = -65.4+36.8\times[K^+]_o$; X-intercept=1.8 mM $[K^+]_o$).

A third and final series of field potential recording experiments was carried out to determine if manipulation of $[K^+]_o$ in the perfusion solution would modify the long-term potentiation of DH_s excitatory neurotransmission that develops in normal ACSF (containing 3.0 mM $[K^+]_o$) following an exposure to FC. The result obtained from every slice (n = 4) studied in this way was consistent and unambiguous (Figure 4.3) – that is, at the time at which the effect of FC on the $P\text{-}PSP_{DR}$ was maximal (at 30 min after the exposure to FC) switch of the perfusion solution to ACSF containing zero K^+ was accompanied by a rapid decrease of the $P\text{-}PSP_{DR}$ to pre-FC (control) values. Clearly, therefore, DH_s excitatory neurotransmission remained exquisitely sensitive to $[K^+]_o$ after the exposure to FC.

The superimposed field potential recordings at the left of Figure 4.4A illustrate a prominent characteristic of field potential recordings obtained from the medial DH_s (e.g., see Ruscheweyh and Sandkuhler, 2003, also Willoughby et al. 2003) – that is, high-frequency and rhythmic postsynaptic neuronal activation is apparent in the response to dorsal root stimulation (gray trace for the 3 response obtained under the same conditions (black traces). Inspection of the single-trial and average across-trial responses recorded under the 3 conditions shows that: (1) exposure to FC not only is followed by a large increase in the magnitude of the average across-trial DH_s field potential (LTP_{FC}), but also by a prominent increase in the synchronous, high-frequency DH_s activation observable in the response to each stimulus; and (2) both the LTP_{FC} and the increased high-frequency activation induced by FC are substantially reduced when the solution perfusing the slice is switched to ACSF containing zero K^+.

The recently published demonstration that $GABA_A$ receptor block reverses the injury-induced sensitization of nociceptor-specific neurons in the DH_s of intact animals (Garcia-Nicas et al. 2006), together with the proposal (Coull et al. 2003) that GABA becomes a postsynaptic excitatory neurotransmitter in the DH_s following peripheral nerve injury motivated us to evaluate the impact, if any, of $GABA_A$ receptor block on the LTP induced by Figure 4.5C. Panel A in Figure 4.5 shows field potential recordings ($P\text{-}PSP_{DRs}$) obtained from the ipsilateral DH_s of an exemplary subject before ("Control"), 30 min after bath application of FC ("after FC"; revealing a prominent LTP_{FC}) and, finally, 30 min after exposure of the same slice to ACSF containing 20 μM bicuculline ("after Bic"; revealing that after exposure to Bic the LTP induced by FC was no longer evident). The plot in panel B shows the time course of the effect of Bic on the LTP induced by exposure to FC (average of data obtained

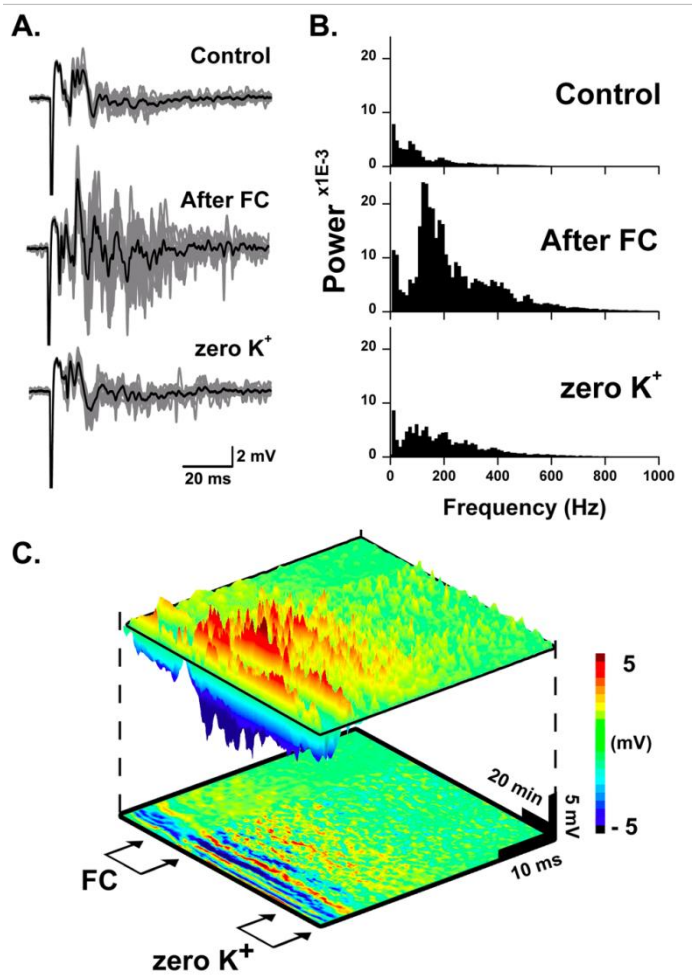

Figure 4.4. Effect of FC on the temporal properties of the DH_s response to dorsal root stimulation. A: Superimposed across-trial (average response to 10 stimuli – black trace) and single-trial responses (gray traces) of DH_s to dorsal root stimulation. Recordings were obtained during the control period (top), 20 min after exposure to FC (middle), and subsequently (bottom) after switch of the perfusion solution to ACSF containing zero K^+. B: Average power spectra computed for all responses (n = 40) obtained during control, after FC, and zero $[K^+]_o$ periods. C: 3D- (top) and surface projection (bottom) maps showing a) synchronous, high-frequency DH_s neuronal activation induced by exposure to FC when $[K^+]_o$ in the ACSF was 3 mM, and b) suppression of the FC-induced high-frequency activation following switch of the perfusion solution to ACSF containing 0 mM K^+.

from 4 slices studied in the same way). Clearly, these findings show that LTP_{FC} depends on $GABA_A$ receptor-mediated neurotransmission because, like its effect on the dorsal horn sensitization induced by application of algesic chemical to the receptive field (Garcia-Nicas et al. 2006), the $GABA_A$ receptor block achieved by Bic antagonizes the LTP induced by exposure to FC.

FFT analysis of the single-trial responses (histograms on Figure 4.4B) quantitatively confirmed that: (1) FC exposure was followed by a prominent increase of the synchronized, high-frequency component of the DH_s response to the dorsal root stimulus; and (2) perfusion of the slice with ACSF containing zero K^+ eliminated the enhancement of the high-frequency component that occurred following the exposure to FC. The pseudocolour 3-D plot (upper part) and surface projection map (lower part) in Figure 4.4C illustrate (for the same slice that yielded the responses in Figure 4.4A) the characteristic temporal attributes of the high-frequency DH_s activation evoked by a dorsal root stimulus following exposure to FC - i.e., multiple peaks in the DH_s field potential; neighboring peaks separated by a 5-8 msec interval during which voltage was at or near-baseline.

The recently published demonstration that $GABA_A$ receptor block reverses the injury-induced sensitization of nociceptor-specific neurons in the DH_s of intact animals (Garcia-Nicas et al. 2006), together with the proposal (Coull et al. 2003) that GABA becomes a postsynaptic excitatory neurotransmitter in the DH_s following peripheral nerve injury motivated us to evaluate the impact, if any, of $GABA_A$ receptor block on the LTP induced by FC. Panel A in Figure 4.5 shows field potential recordings ($P\text{-}PSP_{DRs}$) obtained from the ipsilateral DH_s of an exemplary subject before ("Control"), 30 min after bath application of FC ("after FC"; revealing a prominent LTP_{FC}) and, finally, 30 minafter exposure of the same slice to ACSF containing 20 μM bicuculline ("after Bic"; revealing that after exposure to Bic the LTP induced by FC was no longer evident). The plot in panel B shows the time course of the effect of Bic on the LTP induced by exposure to FC (average of data obtained from 4 slices studied in the same way). Clearly, these findings show that LTP_{FC} depends on $GABA_A$ receptor-mediated neurotransmission because, like its effect on the dorsal horn

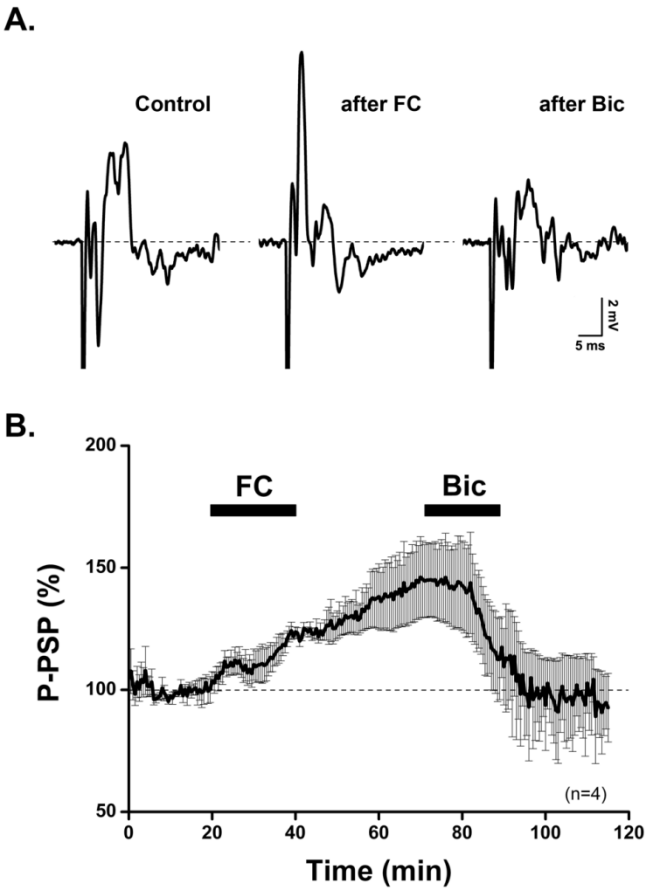

Figure 4.5. *Effect of bicuculline (Bic) on LTP induced by FC.* A: Average of five consecutive field potentials evoked in DH_s by dorsal root stimulus before ("Control"), 10 min after exposure to FC ("after FC"), and after exposure to ACSF containing 20 μM Bic ("after Bic"). B: Plot showing average across-slice (n=4) effect of Bic application on LTP associated with exposure to FC. Error bars indicate ± 1SE.

sensitization induced by application of algesic chemical to the receptive field (Garcia-Nicas et al. 2006), the $GABA_A$ receptor block achieved by Bic antagonizes the LTP induced by exposure to FC.

4.2.2 Cellular-level observations –

4.3.2.1 Effects of FC on the DH_s neuron response to GABA - The current *vs.* time traces in Figure 4.6A show the transmembrane currents evoked at different holding potentials in a representative DH_s neuron in response to the a brief increase in the local concentration of

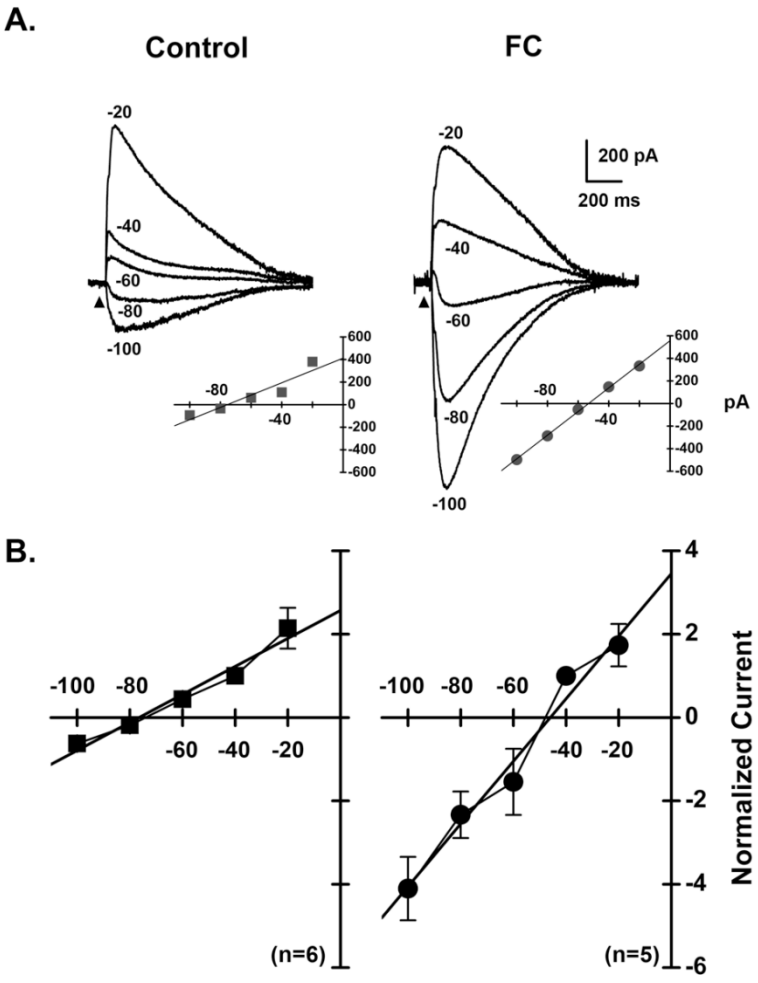

Figure 4.6. *Effect of FC on E_{GABA}.* A: GABA puff-evoked currents recorded from DH_s neuron before and after exposure to FC. A 300 msec puff of 1 mM GABA was applied at each of the indicated holding potentials. E_{GABA} prior to FC was approx. -75 mV; E_{GABA} 20 min after FC was approx. -50 mV. Current-voltage (IV) plots derived from observations obtained from same neuron shown under voltage clamp recordings. B: Plot of normalized average across-neuron I-V plot obtained before (on left; n=6) and after exposure to FC (on right; n=5). Normalization procedure: current measured from each neuron at each holding potential is expressed in terms of the current measured from same neuron/condition at -40 mV. Estimates X-intercept of best fitting linear regression line is -76.5 mV for observations obtained before FC, and -46.1 mV after FC. Flags indicate ±1 S.E.M.

GABA ("puff"), both before ("Control", top left) and after (FC; top right) a 20 min exposure of the slice to 50 μM FC. The I-V curves shown as insets below the traces in Figure 4.6A demonstrate that while the relationship between GABA-evoked peak current and membrane potential is essentially linear both before and after FC, the X-intercept of the best-fitting

linear regression line (indicating the equilibrium potential for the ionic currents triggered by GABA - E_{GABA}) for the observations obtained after the exposure to FC (approx. -50 mV) is substantially more positive than the X-intercept for the data obtained prior to FC (approx. -75 mV).

The left and right panels of Figure 4.6B show I-V curves obtained by averaging the data obtained from 5 neurons studied using the above-described protocol (enabling measurement of peak transmembrane current evoked in each neuron before and after exposure to FC by GABA application at holding potentials stepped between -20 and -100 mV). As was the case for the neuron that provided the data in Figure 4.6A, both the across-neuron (n=5) before-FC (on the left; Figure 4.6B) and after-FC (on the right; Figure 4.6B) I-V curves are well-fit by linear regression lines ($p<.002$), and the X-intercept (indicating E_{GABA}) for the post-FC observations is substantially and statistically different ($p<.001$) from the X-intercept for the pre-FC observations (exposure to FC is associated with a substantial depolarizing alteration – approximately 31 mV - of E_{GABA}; i.e, E_{GABA} changes from -76.5 mV preFC to -46.1 mV postFC). Interestingly (see Discussion), the slope of the regression line for the observations obtained subsequent to FC is significantly larger ($p<.003$) than the slope of the best fitting line for the data obtained prior to FC.

4.3 DISCUSSION

4.3.1 Role of glia in long-term plasticity -

Long-term enhancement of excitatory neurotransmission between small-diameter nociceptive afferents and the DH_s neurons that receive their synaptic terminals (LTP) is regarded as the primary neural mechanism that underlies central sensitization and the

associated abnormalities of pain perception, including hyperalgesia, allodynia, and persistent pain (Sandkuhler, 2000; Woolf and Salter, 2000). Given the use-dependent nature of LTP (Malenka, 1994; Linden, 1997), it is understandable that most studies have employed high-frequency afferent conditioning stimulation to induce it. Nevertheless, the demonstration (Liu and Sandkuhler,1998) that LTP can be induced by spinal application of agents that evoke spike activity in DH_s neurons makes it clear that presynaptic activity is not essential for LTP induction at the initial stage of the CNS pathways that process information about the status of peripheral nociceptors. Instead, it now appears likely (Sandkuhler, 2000) that LTP can result from the extrasynaptic spread of neuroactive compounds synthesized and released by DH_s neurons or glia.

4.3.2 Mechanisms of glial-initiated long-term plasticity -

Although astrocytes normally function as "active partners" in CNS neurotransmission (Newman, 2003), a variety of evidence indicates that under a variety of pathological conditions (peripheral inflammation, injury, infection) their contributions can become maladaptive. The finding (Coull et al. 2003) that nerve injury is accompanied by trans-synaptic reduction in the neuronal expression of the potassium-chloride exporter KCC2 – an alteration that disrupts lamina I neuron anion homeostasis – is notable in this regard because it raises the possibility that abnormal dorsal horn glia-neuron interactions can contribute to hyperalgesia / persistent pain. Coull et al. (2003) demonstrated that DH_s lamina I neuron expression of KCC2 is decreased after nerve injury – an outcome that results in the intracellular accumulation of Cl^- in lamina I neurons which, in turn, shifts the Cl^- equilibrium potential in a depolarizing direction and, in this way, converts the postsynaptic action of GABA from hyperpolarizing (inhibitory) to depolarizing (excitatory).

As a result, after nerve injury DH_s neurons exhibit abnormal excitability including a novel responsivity to peripheral stimuli that evoke activity in A_β afferents (Coull et al. 2003; Garcia-Nicas et al. 2006; Torsney and MacDermott, 2006). Although comparable studies of DH_s neurons remain to be carried out, Fiumelli et al. (2005) have demonstrated that repetitive postsynaptic spiking of hippocampal neurons leads (within minutes) to a Ca^{2+}-dependent downregulation of KCC2 expression, a depolarizing shift of E_{GABA} and, as a consequence, the effect of GABA converts from inhibition to excitation.

Although significant gaps (such as the effect of spike activity on KCC2) remain to be addressed, the findings obtained in the present study significantly extend current views of the mechanisms by which DH_s excitatory neurotransmission undergoes modification. First, they demonstrate that the elevation of local $[K^+]_o$ that occurs in the DH_s subsequent to inhibition of astrocyte energy metabolism by FC is accompanied by a depolarizing shift in the E_{GABA} of DH_s neurons (Figure 4.6A and B) which converts the effect of the transmembrane ionic currents associated with $GABA_A$ receptor activation convert from hyperpolarizing (inhibitory) to depolarizing (excitatory). Second, the observations obtained in the present study reveal that exposure to FC is accompanied by a significant increase in the slope of the relationship between membrane potential and the transmembrane current evoked by GABA (Figure 4.6) – an outcome indicates that DH_s neurons exhibit a larger GABA-mediated membrane conductance to Cl^- after exposure to FC (compare current traces obtained before and after FC; Figure 4.6A).

The prominent suppression of the OIS_{DR} that reliably follows exposure to FC (Figure 1) is fully consistent with the proposal that astrocytes are the major source of the tissue transmittance increase that underlies the intrinsic optical signal (OIS_{DR}) evoked in the DH_s by

dorsal root stimulation (reviewed in Lee et al. 2005). This effect of FC, taken together with the report (Svoboda, et al. 1988) that in normal subjects $[K^+]_o$ is maintained at lower values in the superficial dorsal horn (laminae I-II) than in the deeper laminae (laminae III-V), raises the functionally intriguing possibility that the capacity of astocytes to remove excess extracellular K^+ (as well as glutamate and other neuroactive substances) is substantially greater in the DH_s than in the deeper layers of the horn.

4.3.3 A DH_s control mechanism involving astrocyte-neuron interactions -

Although additional evidence will be required to confirm its validity, the view which guides our ongoing investigation of DH_s glial-neural interactions is that astrocytes are part of a DH_s control mechanism which, in normal subjects, permits relatively rapid and effective adjustment (accomplished via stimulus-directed astroctye-neuron interactions) of the excitability/responsivity at this initial stage of CNS nociceptive information processing. The contributions to both normal and abnormal sensory function of such a control mechanism are regarded as potentially significant. More specifically, although the normally highly efficient astrocyte regulation of $[K^+]_o$ in the DH_s ensures the maintenance of a relatively low (presumably desirable) level of excitability at this initial level of the CNS "pain" projection path, the slow (relative to stimulus-driven neuronal activity) temporal characteristics of DH_s astrocyte-mediated uptake and release of K^+ and other neuroactive substances may contribute importantly to experience-driven and functionally-adaptive modulation of DH_s neuron responsivity (e.g., these properties of DH_s astrocytes may enable astrocytes to modify the "wind-up" behavior of DH_s neurons). Finally, a vigorous episode of nociceptor afferent input (e.g., that evoked by intracutaneous injection of algesic chemical; Lee et al. 2005) is

viewed to make this control system maladaptive by interfering with the ability of DH_s astrocytes to regulate extracellular K^+ and glutamate which, as demonstrated by the experimental findings described in this paper, triggers a long-term enhancement of DH_s excitatory neurotransmission (LTP) that, in a conscious subject, would be accompanied by perceptual abnormalities such as hyperalgesia, allodynia, and persistent pain.

4.3.4 Concepts of glia involvement in spinal cord nociceptive information processing –

Multiple animal behavioral studies have used FC to assess the role of glia in the hyperalgesia that occurs following manipulations such as intracutaneous injection of algesic chemical (e.g, formalin - Watkins et al. 1997; zymosan – Meller et al. 1994), tetanic electrical stimulation of a peripheral nerve at C-fibre strength (Ying et al. 2006; Ma and Zhao, 2002), or perisciatic application of agents that evoke immune activation (Chacur et al. 2001). Such studies have consistently reported that direct application of FC to the spinal cord (e.g., at 10 min – 1 hr before performance of the manipulation used to elicit hyperalgesia) at a dose that inhibits glial energy metabolism via the TCA cycle prevents or greatly attenuates the hyperalgesia - and this effect of FC has uniformly interpreted to indicate that the FC inhibition of glial metabolism prevents the glial release of a variety of factors critical for the excessive activation of dorsal horn neurons that underlies hyperalgesia.

This interpretation appears directly at odds with this study's finding that transient exposure to FC induces a long-term enhancement of excitatory neurotransmission in the superficial spinal cord dorsal horn. Consideration of our observations in the context of those reported in a recent study of hippocampal neuron-astrocyte metabolic interaction (Bacci et al. 2002), however, suggests an alternative and, at least to date, not previously considered

explanation for the finding that spinal pre-administration of FC prevents/attenuates the hyperalgesia induced by intracutaneous injection of algesic chemical, peri-sciatic immune activation, or tetanic stimulation of C-fibre afferents. That is, Bacci et al. (2002) found that exposure to FC not only inhibits astrocyte energy production via the TCA cycle, but also leads FC-intoxicated astrocytes to use glutamine as an alternative energy source, enabling astrocyte ATP levels to be maintained near-to-normal for hours (for concise review of effects of FC on astrocyte energy metabolism see Bacci et al. 2002). As a result, as astrocyte release of glutamine declines in the presence of FC, primary afferent nerve terminals become deprived of the glutamine required to maintain the efficacy of excitatory glutaminergic neurotransmission between nociceptive afferents and DH_s neurons, dorsal horn nociceptive information processing fails, and pain perception diminishes. Accordingly, although behavioral studies have shown that prior FC application to the spinal cord prevents/attenuates hyperalgesia, this effect of FC may not be attributable (as has been widely assumed) to astrocyte release of neuroactive substances, but instead may be the result of a decreased availability of astrocytic glutamine for conversion to glutamate in primary nociceptive afferent terminals (via the glutamine-glutamate cycle; Bacci et al. 2002; Lee et al. 2005; Largo et al. 1996). The rapid onset of the DH_s neuron LTP that occurs after washout of FC is regarded as consistent with this interpretation. In addition, our finding that LTP_{FC} is reduced/eliminated by lowering K^+ in the soluFigure 4.4tion perfusing the slice (Figure 4.2) is viewed to indicate that DH_s $[K^+]_o$ increases when astrocyte metabolism is inhibited, and contributes importantly (via direct actions on neurons and/or by enhancing NMDA receptor activity) to the long-term enhancement of DH_s excitatory neurotransmission observed subsequent to exposure to FC.

Chapter 5

Contribution of GABA to cerebral cortical dynamics

5.1 Background

GABAergic synaptic transmission mediated by $GABA_A$ receptors is the main source of inhibition in the cerebral cortex. In the immature neonatal cortex $GABA_A$-mediated synaptic transmission is excitatory, but in the adult cortex it becomes inhibitory due to a reversal of Cl^- concentration gradient across the neuronal membrane, which is brought about by developmental changes in the expression of anion co-transporters, resulting in lowering of $GABA_A$ reversal potential (E_{GABA-A}) below the resting membrane potential (Voipio and Kaila 2000; Rivera et al. 2005). However, even in the adult cortex $GABA_A$-mediated action can be excitatory in some circumstances. In particular, because of uneven distribution of Cl^- ion channels, E_{GABA-A} is substantially higher in dendrites of pyramidal neurons than in their somata, and as a result a local GABA release at distal dendrites can have a depolarizing effect on the neuron's membrane potential (Gulledge and Stuart 2003). Also excitatory can be the effect of GABA release by chandelier cells at their synapses on the initial axon segments of pyramidal cells, due to the elevated presence of Cl^- ion channels there (Woodruff and Yuste 2008).

Even GABA released at somata of pyramidal cells can become excitatory, which can happen in local neuronal populations subjected to tetanic stimulation, which produces a shift in Cl^- concentration inside the cells and a rise of E_{GABA} (Fujiwara-Tsukamoto et al. 2007).

Such a tetanically-induced reversal of GABA effect has been most thoroughly studied in hyppocampal slices, although Kaneda et al. (2005) reported similar effects of tetanic stimulation in temporal cortical slice as well.

An indirect evidence of a significant contribution of GABA reversals to normal neocortical functioning also comes from Whitsel et al. (2010) study of the response of neurons in area 3b of the primary somatosensory cortex (SI) to vibrotactile skin stimulation in the presence of noxious skin stimulation. That study suggested that in SI cortical columns that are strongly driven by vibrotactile stimulation GABA becomes less inhibitory, or can even become excitatory.

In this paper we show directly – by measuring electrically and optically the effect of GABA release on neurons' membrane potential – that GABA can become depolarizing in somatosensory cortical columns that are driven by afferent stimulation at intensities representative of those experienced in normal life. We also show that such a reversal of GABA action is associated with accumulation of Cl^- and Ca^{2+} within the active neurons. Finally, we show that GABA reversal has the effect of funneling stimulus-evoked activity in a cortical area into spatially confined cortical columns.

5.2 BASIC EXPERIMENTAL SETUP

The basic experimental design for evaluating the effect of GABA on neurons in stimulus-activated cortical columns is illustrated in Figure 1. Activity of a cortical column in a somatosensory cortical slice was produced by local electrical stimulationat the border between layer VI and white matter via a circular bipolar electrode. Such stimulation mimics sensory stimulus-evoked thalamic afferent drive on a cortical column; it evokes

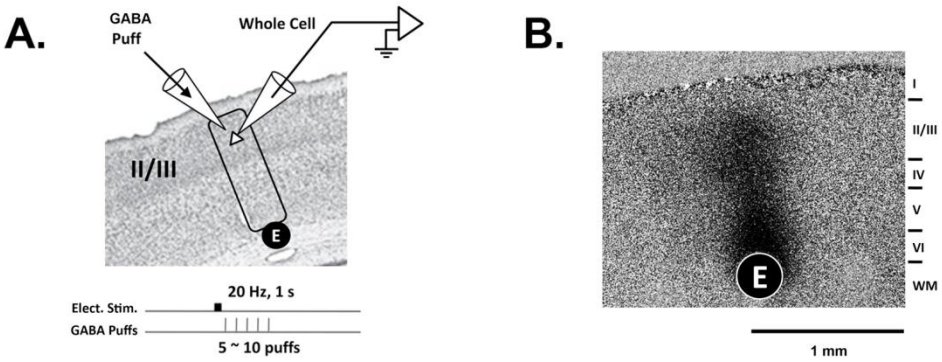

Figure 5.1. Experimental design. A: Schematic diagram of the experimental setup, showing the placement of a circular bipolar stimulating electrode at the layer VI/white matter junction; a cortical column-shaped region activated by electrical stimulation through that electrode; a pyramidal cell (shown as a triangle) isolated with a whole cell patch clamp recording electrode; and a GABA-containing micropipette with a tip in a close proximity to the recorded neuron. GABA is repeatedly pressure-ejected from the micropipette following a brief period of electrical titanic stimulation of the slice. B: Representative example of an OIS response to electrical titanic stimulation (200μA electrical pulses delivered at 20Hz), revealing activation of a column-shaped cortical region.

neuroelectrical activity in a ~300μm diameter column-shaped cortical region that spans layers II-VI (Figure 1A). The spatial extent of the activated cortical column was visualized by imaging optical intrinsic signal (OIS) evoked by the stimulus (Figure 1B). Next, an upper-layer neuron in the center of the OIS-imaged cortical column was picked for whole-cell patch recording. GABA was released at the neuron's soma by pressure-ejecting it from a glass pipette whose tip was guided under microscope to within 50-100μm from the soma. The effect of the released GABA on the cell's membrane potential was measured at the rest (control) and also immediately following a 1s-long period of electrical stimulation of the host cortical column through the layer VI/white matter electrode.

5.3 RESULTS

5.3.1 Reversal of GABA action by the preceding stimulus-evoked activity

We confined our study of GABA effects to the most numerous class of neocortical neurons; i.e., the Regular Spiking (RS) neurons. Whole-cell patch-clamp recorded neurons were identified as RS on the basis of their spike frequency accommodation. An exemplary study of one representative RS neuron is illustrated in Figure 5.2. After placing a stimulating

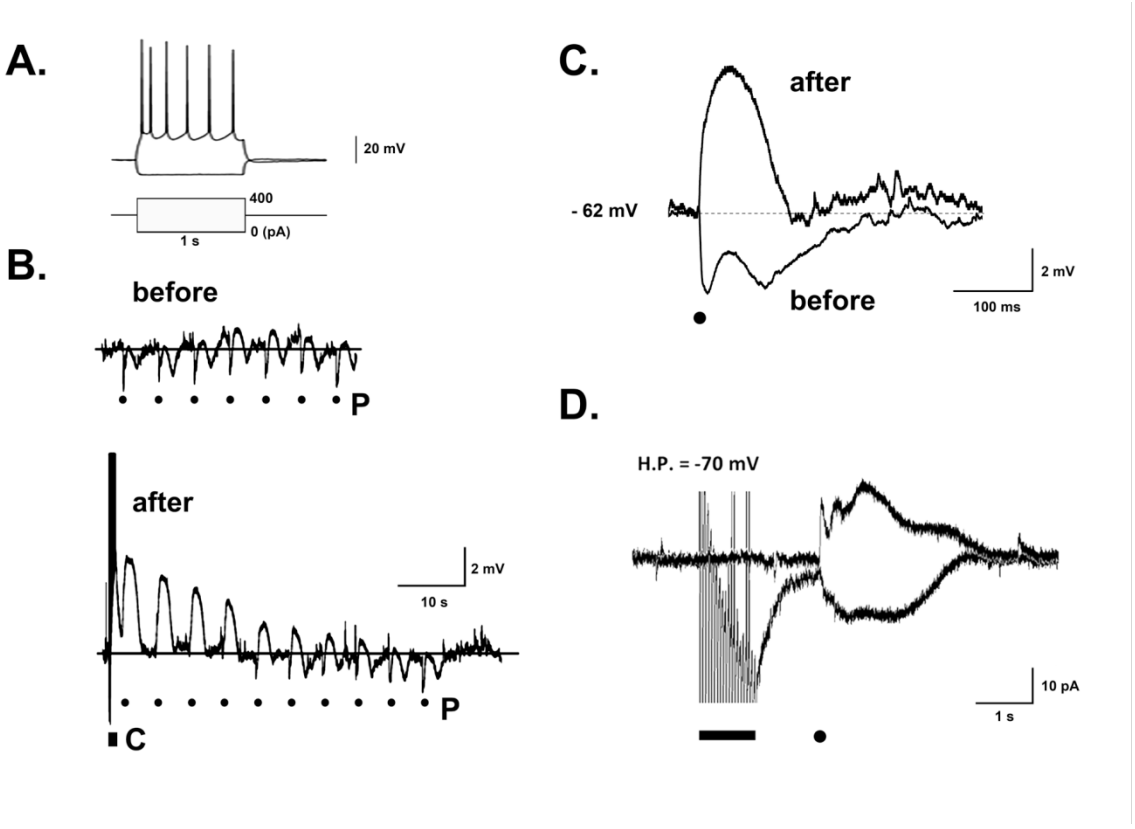

Figure 5.2. Reversal of GABA effect on the membrane potential of a representative RS neuron by the preceding stimulus-evoked activity. A: Membrane depolarization-induced spike firing pattern of the isolated neuron, exhibiting frequency adaptation characteristic of RS neurons. B: Time-course of the neuron's membrane potential during a period when puffs of GABA (P-labeled black circles) were released at the neuron's soma before (top trace) and immediately after (bottom trace) electrical stimulation (C-labeled black rectangle). C: Time-course of depolarizing membrane potential response to the first GABA puff after electrical stimulation vs. the hyperpolarizing time-course of GABA puff response before electrical stimulation (average over 7 puffs shown in panel B). D: Voltage clamp recording showing movement of GABA-mediated currents with and without conditioning stimulation. Black bar and filled triangle indicate timing of applied electrical stimulation and GABA puff.

electrode at the layer VI/white matter border and imaging OIS responses of the slice to 1s-long trains of 20 electrical pulses delivered through that electrode, an upper-layer RS neuron was isolated in the center of the electrode-activated cortical column. Figure 5.2 shows whole-cell patch-clamp recordings obtained from that cell under varying conditions.

To study the effects of GABA on this neuron, the tip of a GABA-containing micropipette was placed under microscope guidance at ~70μm distance from the cell's soma. Puffs of GABA were pressure-ejected from the pipette while recording the cell's membrane potential in the current-clamp mode. Figure 5.2B shows the membrane potential trace during a period when a series of 7 GABA puffs were released while the slice was in its resting state. As Figure 5.2B shows, these exogenous GABA puffs had a prominent hyperpolarizing effect on the cell membrane potential. To make clear the waveform of the cell's response to a GABA puff, the membrane potential traces evoked by each GABA puff are superimposed in Figure 5.2C, revealing a clearly multi-phasic hyperpolarizing response. The shape and the duration of this response well reproduce those reported by others (Collin et al. 1995; Kaila et al. 1997; Martina et al. 2001).

In contrast to such hyperpolarizing effect at rest, GABA puffs released closely following a bout of vigorous locally evoked neuroelectrical activity have an opposite, depolarizing effect. That is, we activate the cortical column within which the recorded neuron resides by delivering a 1s-long train of 20 electrical pulses through the layer VI stimulating electrode, just as we did to evoke the OIS responses. Immediately after this "conditioning" train of electrical pulses, we release a series of 10 puffs of GABA, one every 5s, starting 2s after the end of electrical stimulation. As shown in Figure 5.2D, the first few GABA puffs prominently depolarize – rather than hyperpolarize (as seen in Figure 5.2B) – the cell

membrane potential. The amplitude of this puff-evoked depolarization gradually declines with each successive GABA puff until after 7-8 puffs the response to puffs returns to its original hyperpolarizing form observed in the un-stimulated slice.

To observe GABA-evoked transmembrane currents, the same neuron was also studied in a voltage-clamp mode, holding the membrane potential at -70mV. As is shown in Figure 5.2E, GABA puffs applied to the neuron in the resting, un-stimulated slice trigger typical inward currents. In contrast, when GABA puffs are applied immediately following a 1s-long period of 20Hz electrical stimulation of the cortical column, these puffs trigger currents in the opposite, outward direction.

Overall, the effect of conditioning stimulation on GABA action was studied in 16 RS neurons isolated in the upper cortical layers. Responses of all 16 studied cells to a train of GABA puffs are plotted together in Figure 5.3A. The figure shows that whereas in a resting cortical slice GABA puffs had consistently a hyperpolarizing effect on the cells' membrane potential (shown as black dots), immediately following a 1s period of conditioning electrical stimulation GABA puffs had consistently a depolarizing effect on the cells' membrane potential (shown as open triangles). This effect of conditioning stimulation on the polarity of GABA action is only transient. Each successive GABA puff following conditioning stimulation produces less and less depolarization of the cells' membrane potential and eventually returns to the original (resting) hyperpolarizing response.

To map the average time-course of the effect of conditioning stimulation on GABA action, the distributions of the resting and post-conditioning GABA puff responses of the 16 studied neurons were fitted with 2^{nd} order polynomials, which are plotted in Figure 5.3B.

Also plotted in Figure 5.3B is the difference of the two polynomials, revealing the time-course of the conditioning effect lasting close to 28s.

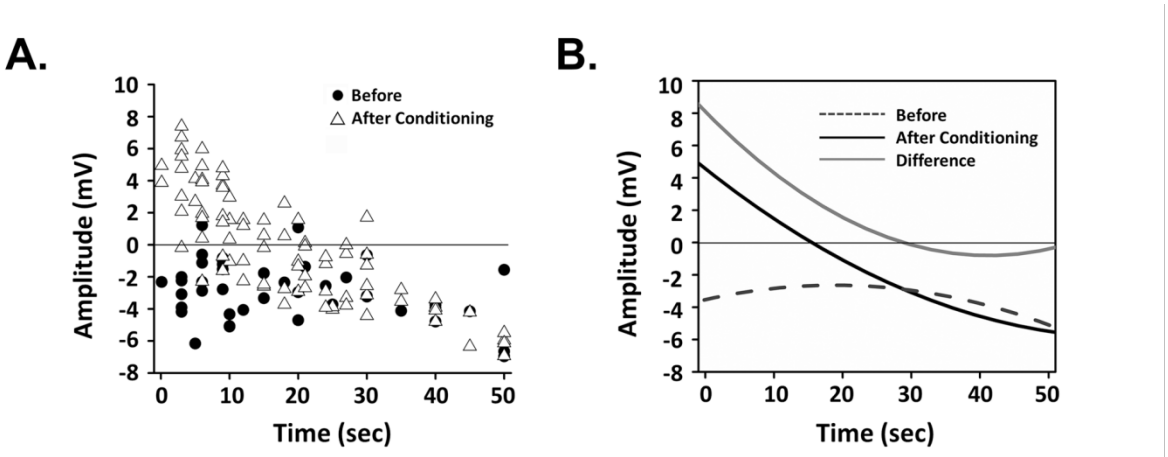

Figure 5.3. Responses of 16 upper-layer RS neurons to a train of GABA puffs. A: Amplitude of each cell's membrane potential response to GABA puffs is plotted as a function of time of puff delivery in the train. Shown are responses to GABA puffs before (black circles) and after (open triangles) conditioning stimulation. B: Second-order least-squares approximations of the before- and after-conditioning distributions of GABA responses in panel A, together with their difference, revealing the time-course of the effect of conditioning electrical stimulation on postsynaptic GABA action.

5.3.2 Accumulation of Cl^- in pyramidal neurons during conditioning stimulation

GABA-mediated excitation might be due to an activity-dependent shift of the $GABA_A$ reversal potential, E_{GABA-A} (Gardner and Spencer 1972; Poolos et al. 1987; Fujiwara-Tsukamoto et al. 2007; Bannai et al. 2009). $GABA_A$-receptor mediated channels are permeable to Cl^- and HCO_3^- ions. E_{GABA-A} is primarily determined by Cl^-, because the permeability of Cl^- is five times that of HCO_3^-. During vigorous neural activity produced by our conditioning stimulation, influx of Cl^- and efflux of HCO_3^- through opened $GABA_A$ ionophores can be expected to lead to an accumulation of Cl^- inside neurons and an accumulation of HCO_3^- outside. To test whether our 1s-long 20Hz conditioning stimulation does lead to accumulation of Cl^- in the activated neurons, we used a genetically modified

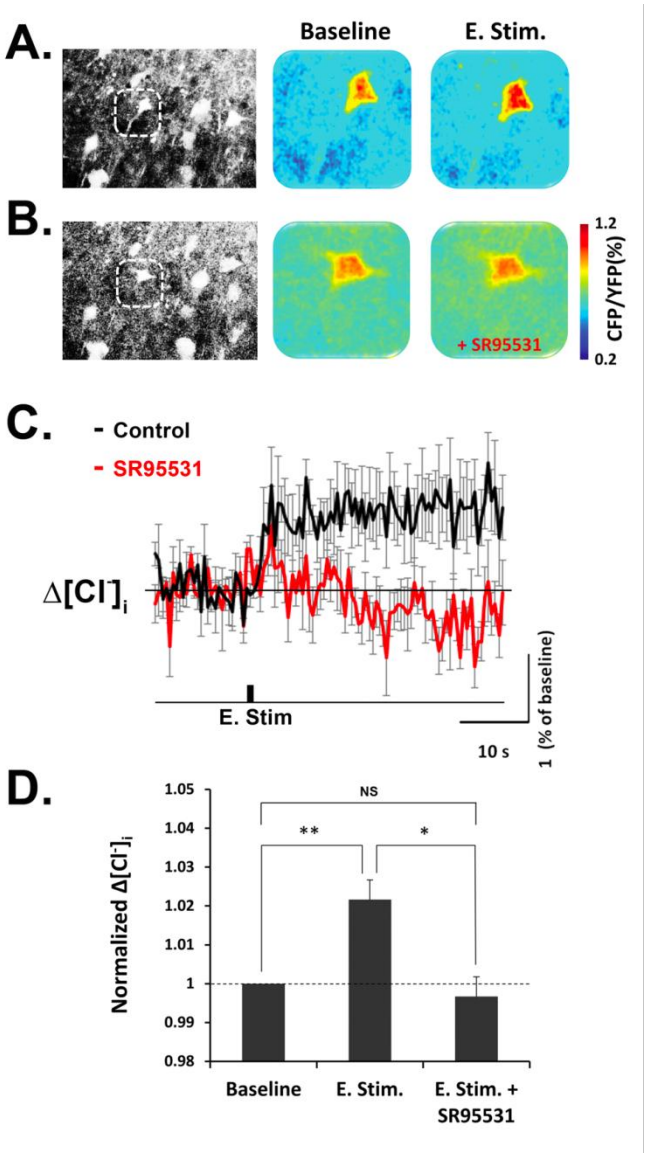

Figure 5.4. 2-photon Cl^- imaging in Clomeleon mouse cortical slice. A: Single-cell Cl^- imaging, showing that concentration of Cl^- within a selected upper-layer pyramidal neuron (identified by a box) is greater after conditioning electrical stimulation (E. Stim.) than before (Baseline). Images are averages of 15 consecutive frames. B: Cl^- imaging of the same neuron as in A, but taken in the presence of $GABA_A$ receptor antagonist SR95531, showing that with $GABA_A$ channels blocked, conditioning electrical stimulation had no effect on $[Cl^-]_i$ in the cell.
C: ??????
D: Average $[Cl^-]_i$ during 10s following the onset of conditioning stimulation, normalized by $[Cl^-]_i$ before stimulation (baseline). Shown are the average values obtained in the presence and absence of $GABA_A$ antagonist SR95531 in 4 slices. ** - $P < 0.001$; * - $P < 0.05$; NS – not significant.

Clomeleon mouse strain, which makes possible selective Cl^-ion imaging at high resolution within the physiological range of ion concentrations and time scale. With cortical slices taken

from Clomeleon mice, we monitored change of FRET signals under 2-photon microscopy before and after conditioning stimulation, using CFP:YFP ratio as an indicator of change of concentration of Cl^- inside the cells. Under 2-photon imaging, we observed brief elevation of $[Cl^-]_i$ in individual upper-layer pyramidal neurons following conditioning electrical stimulation of the cortical column within which those neurons reside (Figure 5.4A). This stimulation-induced increase of $[Cl^-]_i$ in pyramidal neurons was completely blocked when 10mM of a selective $GABA_A$ receptor blocker SR95531 (gabazine) was added to ACSF in the recording chamber (Figure 4B and C). Overall, the effect of conditioning stimulation on $[Cl^-]_i$ was tested in 4 cortical slices taken from 4 mice and summarized in Figure 4D. Both the elevation of $[Cl^-]_i$ due to conditioning stimulation and the suppression of this elevation by $GABA_A$ blocker SR95531 were found to be statistically significant, thus indicating that an excessive influx of Cl^- into the cells through $GABA_A$ channels during robust thalamocortical afferent drive might be responsible, at least in part, for elevation of $E_{GABA\text{-}A}$ and the observed depolarizing effects of GABA puffs immediately after conditioning stimulation.

5.3.3 Post-conditioningly, $GABA_A$ mediates Ca^{2+} influx into pyramidal neurons

Intracellular Ca^{2+} concentration, $[Ca^{2+}]_i$, is widely used as an efficient noninvasive indicator of membrane depolarization in single neurons and in entire neuronal populations. Thus we used $[Ca^{2+}]_i$ imaging as an alternative means of testing whether vigorous neuroelectrical activity in a cortical column can reverse the polarity of GABA action, so that it will depolarize, rather than hyperpolarize, postsynaptic neurons. We stained cortical slices with Fura-2AM, Ca^{2+} indicator, and recorded Ca^{2+} signals in pyramidal neurons using 2-photon microscopy under 20× magnification (Figure 5).

Figure 5.5A shows two representative Fura2-AM stained neurons. At first they were imaged following our standard (1s 25Hz) conditioning electrical stimulation of the cortical column in which they reside, revealing some influx of Ca^{2+} into the cells (top panel). Next, the same two cells were imaged following the same conditioning electrical stimulation coupled with a switch to ACSF containing 10μM $GABA_A$ agonist isoguvacine, which was performed within 2s after the electrical stimulation. As the bottom panel in Figure 5.5A shows, in the presence of $GABA_A$ agonist the two cells acquired noticeably greater post-stimulation $[Ca^{2+}]_i$.

Figure 5.5B shows the time-course of stimulation-induced $[Ca^{2+}]_i$ changes in 8 upper-layer neurons studied in cortical slices that came from 4 different mice. $[Ca^{2+}]_i$ was monitored at a single-cell resolution by integrating the signal over the cell body area in each image frame (images were taken xx s apart). The top panel in Figure 5.5B shows a minor transient (<20s) increase in $[Ca^{2+}]_i$ in the majority of the studied cells following 1s of 25Hz

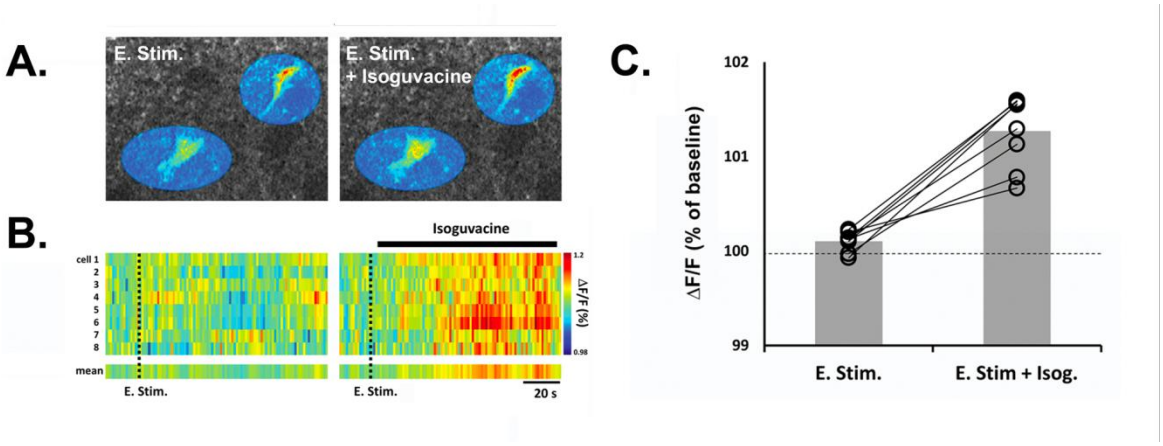

Figure 5.5. Single-cell 2-photon Ca^{2+} imaging in Fura-2AM stained cortical slices. A: Two representative Fura-2AM stained upper-layer pyramidal neurons imaged for x sec starting y sec after conditioning electrical stimulation in normal ACSF (left panel) and in ACSF containing $GABA_A$ agonist isoguvacine (right panel). B: Time-course of stimulation-induced $[Ca^{2+}]_i$ changes in 8 upper-layer pyramidal neurons imaged in normal ACSF (left) and in the presence of 10μM isoguvacine (right). C: Time-averaged post-stimulation change in $[Ca^{2+}]_i$ in the 8 neurons plotted in B. Fura-2AM signal was averaged over x sec beginning y sec after the end of stimulation.

conditioning electrical stimulation. In contrast (see the bottom panel), when the conditioning stimulation was followed within 2s by a switch to isoguvacine-containing ACSF, it provoked a much greater and longer lasting elevation of $[Ca^{2+}]_i$. Figure 5C plots the time-averaged post-stimulation change in $[Ca^{2+}]_i$ in each of the 8 studied neurons in the presence vs. absence of $GABA_A$ agonist isoguvacine, showing that isoguvacine elevates $[Ca^{2+}]_i$, thus suggesting that it depolarizes neurons in the stimulated cortical column.

To determine the spatial extent of the effect of conditioning stimulation of a cortical column on GABA action, we imaged Ca^{2+} signals in Fura-2AM stained cortical slices using 2-photon wide-view microscopy under 4× magnification (Figure 5.6). To show the spatial distribution of Ca^{2+} signal across the slice, a 1.2mm long region was selected in the slice at the level of layers II/III above the layer VI stimulating electrode and partitioned into 8 150μm-wide box-shaped regions of interest, ROI (Figure 5.6A). Average Fura-2AM intensity within each ROI was computed in each successive image frame taken around the time of the delivery of conditioning stimulation and plotted in Figure 5.6A as a time series. A comparison of the time-series plots in Figure 5.6A obtained in the presence vs. absence of isoguvacine shows that exposure to isoguvacine led to a marked increase in Ca^{2+} signal, especially in those ROIs that lie closest to the layer VI stimulating electrode.

This effect of isoguvacine on Ca^{2+} signal is quantified in Figure 5.6B, which plots the average Fura-2AM intensity in each ROI during xx sec following conditioning stimulation. This plot suggests that isoguvacine had a substantial facilitatory effect on Ca^{2+} signal within a 300-400μm wide cortical column centered on the layer VI stimulating electrode.

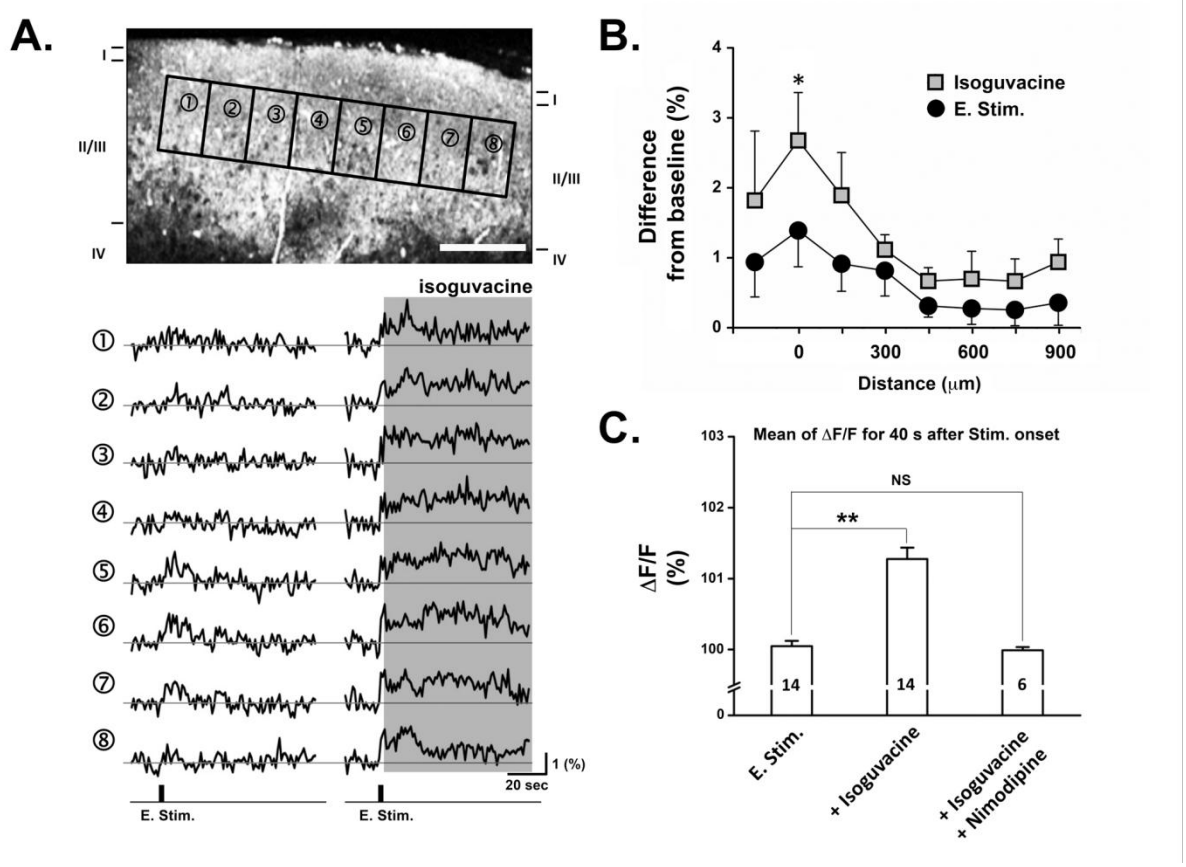

Figure 5.6. Population-scale 2-photon Ca^{2+} imaging in Fura-2AM stained cortical slices. A: Spatiotemporal distribution of stimulation-evoked Ca^{2+} signal across 1.2mm upper-layer cortical region above a stimulating electrode placed at the layer VI/white matter junction. Shown above is a view of a cortical slice at the level of its upper layers, partitioned into 8 box-shaped regions (ROI). Shown below are Ca^{2+} traces measured in each of the 8 boxes around the time of conditioning electrical stimulation in the normal ACSF (left) and in the presence of isoguvacine, which was released into the recording chamber 2s after conditioning stimulation (shaded area in the right-side plot). B: Average (n = 4 slices) stimulation-evoked Ca^{2+} signal measured in each ROI during xx sec following conditioning stimulation in the presence (gray squares) or absence (black circles) of isoguvacine in the ACSF. ROIs in different slices were aligned so that the second from the left ROI is the one with the highest Fura-2AM intensity in the absence of isoguvacine (control).

Finally, Figure 5.6C shows that when isoguvacine was released into the recording chamber together with 2mM nimodipine, which is an L-type Ca^{2+} channel blocker, isoguvacine failed to elevate Ca^{2+} signal following conditioning stimulation. These results indicate that release of isoguvacine in an active cortical column can lead to Ca^{2+} influx into neurons through L-type Ca^{2+} channels.

5.3.4 GABA action in an active cortical column can be both excitatory in the center and inhibitory in the margins

Figure 5.6C suggests that a change of the polarity of GABA action from hyperpolarization to depolarization is confined to the center of a vigorously stimulated cortical column, while at its margins GABA remains hyperpolarizing. We tested this hypothesis directly by imaging stimulus-evoked OIS activity in a cortical slice in the presence vs. absence of $GABA_A$ antagonist bicuculline (BIC). Figure 7 shows the results of a representative experiment. During the experiment OIS was imaged in a somatosensory cortical slice in response to 1s of supra-threshold (3mA) 25Hz electrical stimulation applied via a circular bipolar electrode at the layer VI/white matter border. Such stimulation trials were repeated 9 times, once every 5min. After the first two stimulation trials (which served as a control), ACSF in the recording chamber was switched to ACSF containing 2μM of BIC, so that the last 7 trials were done with a reduced $GABA_A$-mediated synaptic transmission.

Figure 5.7A shows the OIS response to the test stimulation before BIC exposure (left panel) and after 30min of BIC exposure (right panel), revealing a broader, less focused spread of stimulus-evoked OIS activity in the upper cortical layers in the presence of BIC. The spatial distribution of stimulus-evoked OIS activity across the upper layers is plotted in Figure 7B for both the control (black line) and BIC (gray line) conditions. Also plotted in Figure 5.7B is the difference between the two curves. These plots show that blockade of $GABA_A$ receptors by BIC had opposite effects in the center of the stimulus-activated cortical region vs. its margins. That is, in the most strongly stimulus-driven cortical region BIC reduced the OIS response, whereas in the less well driven cortical regions on both sides of the maximally responsive region BIC elevated the OIS response.

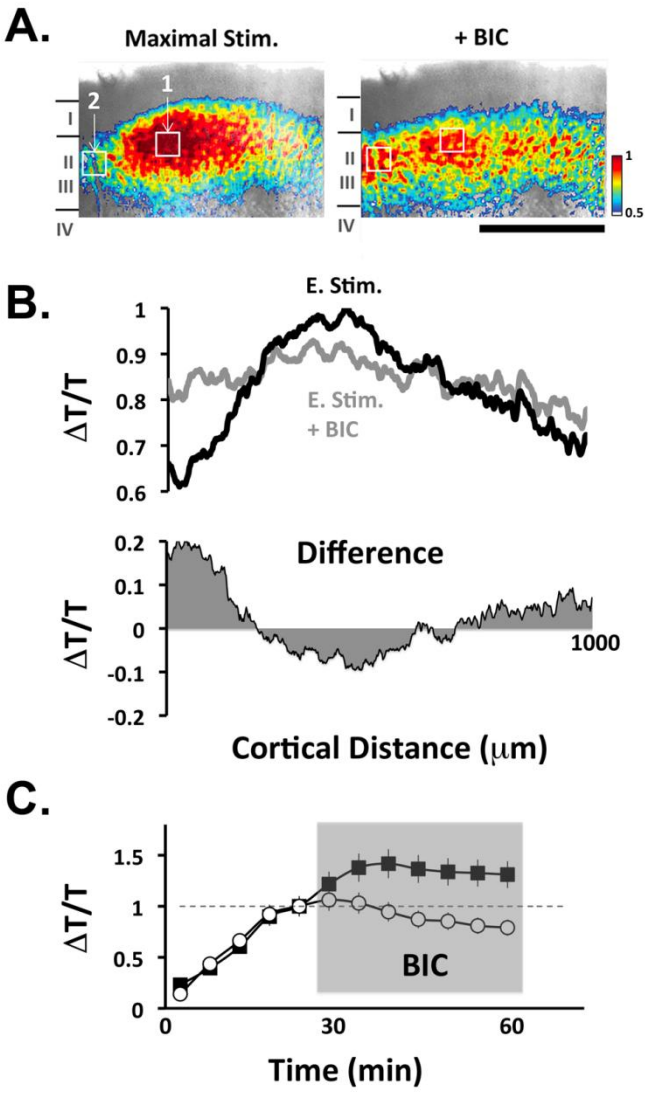

Figure 5.7. Effect of bicuculline (BIC) on spatiointensive pattern of cortical OIS response to conditioning electrical stimulation.
A: Comparison of OIS induced intensive electrical stimulation in the presence of BIC. B: Segmental analysis cross horizontal line in upper layer. Dark line is from intensity of electrical induced OIS and gray line is from electrical induced OIS with BIC. Difference between two lines shows in below. C: Time course of effect of BIC on high stimulus induced OIS. Stimulus intensity of first 3 data point is 0.2, 1.0 and 2.0 mA each. Stimulus intensity from 4th data point to rest of them is 3 mA. All data point normalized by 4th data point to be compared the spatial characteristics of OIS on $GABA_A$ receptors. Filled squares are ROI 2 (margin area) and open circles are ROI 1 (center area).

Similar results were obtained in other cortical slices taken from three additional rats. Figure 7C plots the overall time-course of BIC effect averaged over all four experiments of this series. This plot was produced by selecting in each slice two 50×50 pixel regions of interest (ROI). One ROI boxed-in the site of the maximal BIC-free OIS response to the test electrical stimulation (labeled as box 1 in Figure 5.7A). In each of the four experiments, the average OIS magnitude in the box was measured at each of the 9 stimulation trials and normalized by the magnitude at the last control trial (just prior to BIC release). This sequence of 9 time points, averaged over 4 experiments, is plotted in Figure 5.7C as an open-circle-labeled curve. The second ROI was placed in a marginally responding cortical region (labeled as box 2 in Figure 5.7A). The average OIS magnitude in this box was also measured at each of the 9 test stimulation trials, normalized by the magnitude at the last control trial, and plotted as a time series (averaged over 4 experiments) in Figure 5.7C. The two curves in Figure 5.7C show that once the slice was switched to BIC-containing ACSF, the stimulus-evoked response in the maximally activated cortical region (box 1) gradually declined over 30min to 80% of its response in the absence of BIC. In contrast, the stimulus-evoked response in the marginally activated cortical region (box 2) gradually increased to 130% of its response in the absence of BIC.

Taken together, the OIS observations in Figures 5.7 reinforce our hypothesis – advanced in this paper on the basis of the neurophysiological recordings and Cl^- and Ca^{2+} imaging – that synaptically released GABA can be either inhibitory or excitatory, depending on the activity state of the local network. As Figure 5.7 shows, this activity dependence of GABA action results in funneling of stimulus-evoked activity into the central, most strongly driven cortical columns.

5.4 DISCUSSION

In this series of experiments we examined the effect of GABAergic synaptic transmission on the neocortical pyramidal neurons at rest and immediately thalamic afferent drive evoked by intensive repetitive electrical stimulation of cortical slices taken from 3-4 week old rats and mice. Using electrophysiological and optical imaging approaches we demonstrated :(1) with whole-cell patch-clamp recordings from single neurons, the activity dependency of the direction of GABA action on membrane potential of upper-layer cortical neurons; (2) with two photon imaging stimulus-evoked accumulation of Cl^- in neurons in the clomeleon mouse slice and spatial distribution of Ca^{2+} signal in the stimulated corticalregion; , and (3) with OIS imaging, the contribution of bipolar GABAergic action to spatial sharpening – funneling – of the response of the somatosensory cortex to local columnar stimulation.

Activity-dependent membrane depolarization by GABAergic transmission in cortical pyramidal neurons

Activity-dependent dual action of GABAergic synaptic transmission has been reported extensively in hippocampal neurons (Fujiwara-Tsukamoto et. al. 2007). The depolarizing action of GABA was observed in afterdischarge of pyramidal neuron induced by highfrequency tetanic stimulation of Schaffer collaterals. The present study confirmes such a dual action of GABA in neocortical pyramidal neurons, showing that the polarity of the effect of GABAergic synaptic transmission in response to exogenous exposure to GABA depends on of the preceding thalamic afferent drive activity (see Figs 2 – 3).

That is, observation in the presence of GABAergic depolarization might be associated

with the presence of activation of thalamocrotical afferent drive because under this condition, the cortical pyramidal neuron in upper layer response to transient GABA application is induced depolarized in the beginning and recovered to its original shape (hyperpolarization); Prior to activation of thalamocortical afferent drive, exogenous GABA application evokes hyperpolarization of neuronal membrane potential, whereas immediately after activation of thalamocortical afferent drive GABA application evokeds depolarization, which gradually – over 30s – recovers to original hyperpolarization.

Cellular mechanisms underlying the excitatory effect of GABAergic transmission on cortical pyramidal neurons

The findings obtained in the present study provide some information about the nature of the cellular mechanisms responsible for the activity-dependent bipolar alteration of the GABA effect on cortical neurons that accompanies thalamocortical afferent drive. Present study suggests that even in adult subjects the alteration of cortical neuron membrane ion flows that accompanies GABA binding to $GABA_A$ receptors is not fixed, but is prominently activity-dependent. For example, even a relatively brief stimulation of thalamocortical afferents leads to Cl^- accumulation in the responding cortical pyramidal neurons, which can alter equilibrium potential of Cl^- (Fig. 4). Elevatio of ECl- can convert the action of GABA on cortical $GABA_A$ receptors from inhibitory/ hyperpolarizing to excitatory/depolarizing, as we confirmed by measurement of influx of Ca^{2+} through voltage dependent calcium channels in layer II-II pyramidal neurons of sensorimotor cortex (Fig. 2-3, 5-6). (For analogous mechanisms proposed for hippocampal pyramidal neurons see Staley et al. 1995; Kaila et al. 1997; Isomura et al. 2003; Stein and Nicoll 2003; Walters 2004; Szabadics et al. 2006; Fujiwara-

Tsukamoto et al. 2007; for pyramidal neurons in temporal neocortex see Kaneda et al. 2005; for overview of the excitatory effects of GABA and their supposed functional meaning see Marty and Llano 2005).

A recent in vivo contribution of activity-dependent GABA action to tactile information processing in somatosentory cortex indication of GABA polarity reversal was suggested for the activity dependent behaviors of somatosensory cortical neurons in squirrel monkey (Whitsel et al. 2010). In that study, a procedure that reliably evokes cutaneous pain in humans noxious heat or intradermal capsaicin injection was shown to decrease mean firing rate (MFR) and degree to which neurons in area 3b of squirrel monkey entrain to a 25-Hz stimulus to the receptive field center when stimulus amplitude is near threshold. In contrast, neuronal MFR and entrainment are either unaffected or enhanced by heat probe contact or intradermal algogen injection when the amplitude of 25-Hz stimulation is suprathreshold. The authors hypothesized the alteration of neuronal response to different intensities of vibrotactile stimulus was caused by activity-dependence of the action of GABA on somatosensory cortical neurons. They proposed the GABA-medicated effect of nociceptive afferent drive on the MFR and the entrainement of responses of neurons to 25-Hz stimulation of the RFcenter changes progressively from suppressive/inhibitory to augmenting/excitatory as stimulus amplitude/intensity is increased from near-threshold to suprathreshold values. Activity-dependent reversal of the effect of GABA on postsynaptic neurons might also underlie the funneling of the spatial response of the somasosensory cortex to vibrotactile stimulation.

Previous studies of spatial funneling in somatosensory cortex have demonstrated interactions of single or multiple inputs across cortical sites that are ‘funneled’ centrally so

that perceived intensity at the central site is enhanced (Chen et. al., 2003; Friedman et. al., 2008; Simon et. al., 2005; Tommerdahl et. al., 2010). However, the mechanism of spatial funneling effect is not well understood. Our experiment of recording spatial distribution of OIS with and without blockage of $GABA_A$ receptors by bicucculine suggests that the activity-dependent dual effect of GABAergic transmission contributes to lateral inhibition and produces a sharpening effect in localization of broad stimulus-evoked distributions of cortical activity (Fig 7).

According to our view, even when stimulus conditions are used that are in normal physiological range, the initial GABA response very rapidly is transformed by influences contributed by exchange of cellular ionic distributions and feedback connections with GABAergic interneurons to a response that converts from inhibitory/hyperpolarizing to excitatory/depolarizing.

REFERENCES

Aguado F, Espinosa-Parrilla JF, Carmona M, and Soriano E. (2002) Neuronal activity regulates correlated network properties of spontaneous calcium transients in astrocytes in situ. *J Neurosci* 22: 9430–9444.

Artola A & Singer W (1987). Long-term potentiation and NMDA receptors in rat visual cortex. *Nature* 347, 69-72.

Asai T, Kusudo K, Ikeda H, Takenoshita M & Murase K (2002). Effect of halothane on neuronal excitation in the superficial dorsal horn of rat spinal cord slices: evidence for a presynaptic action. *Eur J Neurosci.* 15, 1278-1290.

Bacci A, Sancini G, Verderio C, Armano S, Pravettoni E, Fesce R, Franceschetti S & Matteoli M (2002). Block of glutamate-glutamine cycle between astrocytes and neurons inhibits epileptiform activity in hippocampus. *J Neurophysiol* 88, 2302-2301.

Banna NR, Saade NE, Atweh SF, and Suhayl JJ. (1986) Prolonged discharge of wide-dynamic range spinal neurons evoked by formaldehyde injected into their cutaneous receptive fields. *Exp Neurol* 93: 275–278.

Bekar LK and Walz W. (2002) Intracellular chloride modulates A-type potassium currents in astrocytes. *Glia* 39: 207–216.

Berg-Johnsen J, Paulsen RE, Fonnum F, and Langmoen IA. (1993) Changes in evoked potentials and amino acid content during fluorocitrate action studied in rat hippocampal cortex. *Exp Brain Res* 96: 241–246.

Binder DK, Papadopoulos MC, Haggie PM, and Verkman AS. (2004) In vivo measurement of brain extracellular space diffusion by cortical surface photobleaching. *J Neurosci* 24: 8049–8056.

Bliss TVP & Collingridge GL (1993). A synaptic model of memory: Long-term potentiation in the hippocampus. *Nature* 361, 31-39.

Chacur M, Milligan ED, Gazda LS, Armstrong C, Wang H, Tracey KJ, Maier SF & Watkins LR (2001). A new model of sciatic inflammatory neuritis (SIN): induction of unilateral and bilateral mechanical allodynia following acute unilateral peri-sciatic immune activation in rats. *Pain* 94, 231-244.

Chen L, Friedman R, Row A. (2003) Optical imaging of a tactile illusion in area 3b of the primary somatosensory cortex. *Science* (New York, NY) vol. 302 (5646) pp. 881-5

Clarke DD, Nicklas WJ, and Berl S. (1970) Tricarboxylic acid-cycle metabolism in brain. *Biochem J* 120: 345–351.

Coull JAM, Boudreau D, Bachand K, Prescott SA, Nault F, Sik A, De Koninck P & De Koninck Y (2003). Trans-synaptic shift in anion gradient in spinal lamina I neurons as a mechanism of neuropathic pain.

Dickenson AH and Sullivan AF. (1987) Subcutaneous formalin-induced activity of dorsal horn neurons in the rat: differential response to an intrathecal opiate administered pre- or post-formalin. *Pain* 30: 349–360.

Dubuisson D and Dennis SG. (1977) The formalin test: a quantitative study of the analgesic effects of morphine, meperidine and brain stem stimulation in rats and cats. *Pain* 4: 161–174.

Fiumelli H, Cancedda L, & Poo M (2005). Modulation of GABAergic transmission by activity via postsynaptic Ca^{2+} - dependent regulation of KCC2 function. *Neuron* 48, 773-786.

Fleck MW, Palmer AM, & Barrionuevo G (1992). Potassium-induced long-term potentiation in rat hippocampal slices. *Brain Res* 580, 100-105.

Fonnum F, Johnsen A & Hassel B (1997). Use of fluorocitrate and fluoroacetate in the study of brain metabolism. *Glia* 21, 106-113.

Friedman, RM, Chen, LM, and Roe, AW (2008) Responses of areas 3b and 1 in anesthetized squirrel monkeys to single- and dual-site stimulation of the digits. *Journal of Neurophysiology* vol. 100 (6) pp. 3185-96

Fu K-Y, Light AR, and Maixner W. (2000) Relationship between nociceptor activity, peripheral edema, spinal microglial activation and long-term hyperalgesia induced by

formalin. *Neuroscience* 101: 1127–1135.

Garcia-Nicas E, Laird JMA & Cervero F (2006). $GABA_A$ – receptor blockade reverses the injury-induced sensitization of nociceptor-specific (NS) neurons in the spinal dorsal horn of the rat. *J Neurophysiol* 96, 661-670.

Garrison CJ, Dougherty PM, and Carlton SM. (1994) GFAP expression in lumbar spinal cord of naïve and neuropathic rats treated with MK-801. *Exp Neurol* 129: 237–243.

Ge W-P & Duan S (2006). Persistent enhancement of neuron-glia signaling mediated by increased extracellular K^+ accompanying long-term synaptic potentiation. *J Neurophysiol*; DOI: 10.1152/jn.00146.2006

Hantman AW, van den Pol AN, and Perl ER. (2004) Morphological and physiological features of a set of spinal substantia gelatinosa neurons defined by green fluorescent protein expression. *J Neurosci* 24: 836–842.

Hassel B, Bachelard H, Jones P, Fonnum F, and Sonnewald U. (1997) Trafficking of amino acids between neurons and glia in vivo. Effects of inhibition of glial metabolism by fluoroacetate. *J Cereb Blood Flow Metab* 17: 1230–1238.

Hassel B, Paulsen RE, Johnsen A, and Fonnum F. (1992) Selective inhibition of glial cell metabolism in vivo by fluorocitrate. *Brain Res* 576: 120–124.

Heinemann U, Schaible H-G, and Schmidt RF. (1990) Changes in extracellular potassium concentration in cat spinal cord in response to innocuous and noxious stimulation of legs with healthy and inflamed knee joints. *Exp Brain Res* 79: 283–292.

Huang YH, Sinha SR, Tanaka K, Rothstein JD, and Bergles DE. (2004) Astrocyte glutamate transporters regulate metabotropic glutamate receptor-mediated excitation of hippocampal interneurons. *J Neurosci* 24: 4551–4559.

Hulsmann S, Straub H, Richter DW, and Speckmann E-J. (2003) Blockade of astrocyte metabolism causes delayed excitation as revealed by voltage-sensitive dyes in mouse brainstem slices. *Exp Brain Res* 150: 117–121, .

Ikeda H, Ryu P-D, Park J-B, Tanifuji M, Asai T, and Murase K. (1998) Optical responses evoked by single-pulse stimulation to the dorsal root in the rat spinal dorsal horn in slice. *Brain Res* 812: 81–90.

Ikeda H, Stark J, Fischer H, Wagner M, Drdla R, Jager T & Sandkuhler J (2006). Synaptic amplifier of inflammatory pain in the spinal dorsal horn. *Science* 312, 1659-1662.

Janigro D, Gasparini S, D'Ambrosio R, McKann GII, and DiFrancesco D. (1997) Reduction of K^+ uptake in glia prevents long-term depression maintenance and causes epileptiform activity. *J Neurosci* 17: 2813–2824.

Kaila K, Lamsa K, Smirnov S, Taira T, and Voipio J. (1997) Long-lasting GABA-mediated depolarization evoked by high-frequency stimulation in pyramidal neurons of rat hippocampal slice is attributable to a network-driven, bicarbonate-dependent K^+ transient. *J Neurosci* 17: 7662–7672.

Kawahara K, Hosoya R, Sato H, Tanaka M, Nakajima T, and Iwabuchi S. (2002) Selective blockade of astrocytic glutamate transporter GLT-1 with dihydrokainate prevents neuronal death during ouabain treatment of astrocyte/neuron cocultures. *Glia* 40: 337–349.

Keyser DO and Pellmar TC. (1994) Synaptic transmission in the hippocampus: critical role for glial cells. *Glia* 10: 237–243.

Klemm F, Carli G, and Reeh PW. (1989) Peripheral neural correlates of the formalin test in rats. *Eur J Physiol* 414: S42.

Kofuji P and Newman EA. (2004) Potassium buffering in the central nervous system. *Neuroscience* 129: 1045–1056.

Kohn A, Metz C, Quibrera M, Tommerdahl M, and Whitsel BL. (2002a) Functional neocortical microcircuitry demonstrated with intrinsic signal optical imaging in vitro. *Neurosci* 95: 51–62.

Kohn A, Metz C, Tommerdahl M, and Whitsel BL. (2002b) Stimulus-evoked modulation of sensorimotor pyramidal neuron EPSPs. *J Neurophysiol* 88: 3331–3347.

Largo C, Cuevas P, Somjen GG, Martin del Rio R & Herreras O (1996). The effect of depressing glial function in rat brain in situ on ion homeostasis, synaptic transmission, and neuron survival. *J Neurosci* 16, 1219-1229.

Lee J, Tommerdahl M, Metz CB, and Whitsel, BL. (2003) Manipulation of neuron-glia interaction in the superficial dorsal horn of rat spinal cord slice. *Soc Neurosci Abstr* 64: 3.

Lee, J, Tommerdahl, M, Favorov, OV, and Whitsel, BL (2005) Optically recorded response of the superficial dorsl horn: Dissociation from neuronal activity, sensitivity to formalin-evoked skin nociceptor activation. J. Neurophysiol. 94: 852-864.

Linden DJ (1999). The return of the spike: postsynaptic action potentials and the induction of LTP and LTD.

Liu XG & Sandkuhler J. (1998). Activation of spinal N-methyl-D-aspartate or neurokinin receptors induces long-term potentiation of spinal C-fibre-evoked potentials. *Neuroscience* 86, 1209-1216.

Lu Y and Perl ER. (2003) A specific inhibitory pathway between substantia gelatinosa neurons receiving direct C-fiber input. *J Neurosci* 23: 8752–8758.

Ma J-Y & Zhao Z-Q (2002). The involvement of glia in long-term plasticity in the spinal dorsal horn of the rat. *NeuroReport* 13, 1781-1784.

MacFarlane SN and Sontheimer H. (1997) Electrophysiological changes that accompany reactive gliosis in vitro. *J Neurosci* 17: 7316–7329.

Malenka RC (1994). Synaptic plasticity in the hippocampus: LTP and LTD. *Cell* 78, 535-538.

McCall WD, Tanner KD, and Levine JD. (1996) Formalin induces biphasic activity in C-fibers in the rat. *Neurosci Lett* 208: 45–48.

Meeuwsen S, Persoon-Deen C, Bsibsi M, Ravid R, and Van Noort JM. (2003) Cytokine, chemokine and growth factor gene profiling of cultured human astrocytes after exposure to proinflammatory stimuli. *Glia* 43: 243–253.

Meller ST, Dykstra C, Grzybycki D, Murphy S & Gebhart GF (1994). The possible role of glia in nociceptive processing and hyperalgesia in the spinal cord of the rat. *Neuropharmacology* 33, 1471-1478.

Meme W, Ezan P, Venance L, Glowinski J, and Giaume C. (2004) ATP-induced inhibition of gap junctional communication is enhanced by interleukin-1treatment in cultured astrocytes. *Neuroscience* 126: 95–104.

Milligan ED, O'Conner KA, Nguyen KT, Armstrong CB, Twining C, Gaykema R, Holguin A, Martin D, Maier SF, and Watkins LR. (2001) Intrathecal HIV-1 envelope glycoprotein gp120 induces enhanced pain states mediated by spinal cord proinflammatory cytokines. *J Neurosci* 21: 2808–2819.

Muir D, Berl S, and Clarke DD. (1986) Acetate and fluoroacetate as possible markers for glial metabolism in vivo. *Brain Res* 380: 336–340.

Murase K, Saka T, Asai T & Ikeda H (1999). Functional circuitry for the induction of prolonged excitation in the rat spinal dorsal horn. *Eur J Neurosci* 11, 3355-3358.

Murase K, Saka T, Terao S, Ikeda H &Asai T (1998). Slow intrinsic optical signals in the rat spinal dorsal horn in slice. *NeuroReport* 9, 3663-3667.

Newman EA (2003). New roles for astrocytes: Regulation of synaptic transmission. *TINS* 109, 1-7.

Newman EA. (2004) New roles for astrocytes: Regulation of synaptic transmission. *Trends Neurosci* 109: 1–7.

Olsen ML and Sontheimer H. (2004) Mislocalization of Kir channels in malignant glia. *Glia* 46: 63–73.

Parkerson KA and Sontheimer H. (2004) Biophysical and pharmacological characterization of hypotonically activated chloride currents in cortical astrocytes. *Glia*46: 419–436.

Pascual O, Casper KB, Kubera C, Zhang J, Revilla-Sanchez R, Sul J-Y, Takano H, Moss SJ,

McCarthy K & Haydon PG (2005). Astrocytic purinergic signaling occrdinates synaptic networks. *Science* 310, 113-116.

Paulsen RE, Contestabile A, Villani L & Fonnum F (1987). An in vivo model for studying function of brain tissue temporarily devoid of glial cell metabolism: The use of fluorocitrate. *J Neurochem* 48. 1377-1385.

Payne JA, Rivera C, Voipio J & Kaila K (2003). Cation-chloride co-transporters in neural communication, development and trauma. *TINS* 26, 199-206.

Porro CA and Cavazzuti M. (1993) Spatial and temporal aspects of spinal cord and brainstem activation in the formalin pain model. *Prog Neurobiol* 41: 565–607.

Porro CA, Cavazzuti M, Lui F, Giuliani D, Pellegrini M, and Baraldi P. (2003) Independent time courses of supraspinal nociceptive activity and spinally mediated behavior during tonic pain. *Pain* 104: 291–301.

Puig S and Sorkin LS. (1996) Formalin-evoked activity in identified primary afferent fibers: systemic lidocaine suppresses phase-2 activity. *Pain* 64: 345–355.

Rioult-Pedotti MS, Friedman D &Donaghue JP (2000), Learning-induced LTP in neocortex. *Science* 290, 533-536.

Rosenberg PA, Amin S, and Leitner M. (1992) Glutamate uptake disguises neurotoxic potency of glutamate agonists in cerebral cortex in dissociated cell culture. *J Neurosci* 12: 56–61.

Ruscheweyh R & Sandkuhler J (2000). Differential actions of spinal analgesics on mono- versus polysynaptic Aδ-fibre-evoked field potentials in superficial spinal dorsal horn in vitro. *Pain* 88, 97-108.

Ruscheweyh R & Sandkuhler J (2001). Bidirectional actions of nociceptin/orphanin FQ on Aδ-fibre-evoked responses in rat superficial spinal dorsal horn in vitro. *Neurosci* 107, 275-281.

Ruscheweyh R & Sandkuhler J (2003). Epileptiform activity in rat spinal dorsal horn in vitro

has common features wqith neuropathic pain. *Pain* 105, 327-338.

Sandkuhler J (2000). Learning and memory in pain pathways. *Pain* 88, 113-118.

Sandkuhler J & Liu X (1998). Induction of long-term potentiation at spinal synapses by noxious stimulation or nerve injury. *Eur J Neurosci* 10, 2476-2480.

Sandkuhler J, Benrath J, Brechtel C, Ruscheweyh R, and Heinke B. (2000) Synaptic mechanisms of hyperalgesia. *Prog Brain Res* 129: 81–100.

Shoham D and Grinvald A. (2001) The cortical representation of the hand in macaque and human area S-I; high resolution optical imaging. *J Neurosci* 21: 6820–6835.

Simard M and Nedergaard M. (2004) The neurobiology of glia in the context of water and ion homeostasis. *Neuroscience* 129: 877–896.

Somjen GG. (2002) Ion regulation in the brain: implications for pathophysiology. *Neuroscientist* 8: 254–267.

Svoboda J, Motin V, Hajek I & Sykova E (1988). Increase in extracellular potassium level in rat spinal dorsal horn induced by noxious stimulation and peripheral injury. *Brain Res* 458, 97-105.

Sykova E, Vargova L, Kubinova S, Jendelova P, and Chvatal A. (2003) The relationship between changes in intrinsic optical signals and cell swelling in rat spinal cord slices. *NeuroImage* 18: 214–230.

Takahashi Y and Nakajima Y. (1996) Dermatomes in the rat limbs as determined by antidromic stimulation of sensory C-fibers in spinal nerves. *Pain* 67: 197–202.

Takahashi Y, Hirayama J, and Nakajima Y. (2002) Segmental regulation patterns of body surface temperature in the rat hindlimb. *Brain Res* 947: 100–109.
Torsney C & MacDermott AB (2006). Disinhibition opens the gate to pathological pain signaling in superficial neurokinin 1 receptor-expressing neurons in rat spinal cord. *J Neurosci* 6, 1833-1843.

Uvarov P, Ludwig A, Markkanen M, Rivera C & Airaksinen MS (2006). Upregulation of the neuron-specific K^+/Cl^- cotransporter expression by transcription factor early growth response 4. *J Neurosci* 26, 13463-13473.

Volterra A and Bezzi P. Release of transmitters from glial cells. (2002) In *The Tripartite Synapse: Glia in Synaptic Transmission*, edited by Volterra A, Magistretti PJ, and Haydon PG. Oxford, UK: Oxford University Press, p. 164–182.

Walz W. (2000) Role of astrocytes in the clearance of excess extracellular potassium. *Neurochem Int* 36: 291–300.

Walz W. (2002) Chloride/anion channels in glial cell membranes. *Glia* 40: 1–10, .

Waniewski RA and Martin DL. (1998) Preferential utilization of acetate by astrocytes is attributable to transport. *J Neurosci* 18: 5225–5233.

Watkins LR & Maier SF (2002). Beyond neurons: Evidence that immune and glial cells contribute to pathological pain states. *Physiol Rev* 82, 981-1011.

Watkins LR, Martin D, Ulrich P, Tracey KJ & Maier SF (1997). Evidence for the involvement of spinal cord glia in subcutaneous formalin induced hyperalgesia in the rat. *Pain* 71, 225-235.

Willoughby JO, Mackenzie L, Broberg M, Thoren AE, Medvedev A, Sims NR & Nilsson M (2003). Fluorocitrate-mediated astroglial dysfunction causes seizures. *J Neurosci Res* 74, 160-166.

Woolf CJ & Salter MW (2000). Neuronal plasticity: Increasing the gain through pain. *Science* 288, 1765-1768.

Yang Y, Ge W, Chen Y, Zhang Z, Shen W, Wu C, Poo M & Duan S (2003). Contribution of astrocytes to hippocampal long-term potentiation through release of D-serine. *PNAS* 100, 15194-15199.

Ying B, Lu N, Zang Y-Q & Zhao Z-Q (2006). Involvement of spinal glia in tetanically sciatic

stimulation-induced bilateral mechanical allodynia in rats. *Biochem and Biophys Res Comm* 340, 1264-1272.